

A conceptual model for glacial lake bathymetric distribution

Taigang Zhang^{1,2,3}, Weicai Wang¹, Baosheng An^{1,4}

¹State Key Laboratory of Tibetan Plateau Earth System, Environment and Resources (TPESER), Institute of Tibetan Plateau Research, Chinese Academy of Sciences, Beijing 100101, China

²College of Earth and Environmental Sciences, Lanzhou University, Lanzhou 730000, China

³Center for the Pan-Third Pole Environment, Lanzhou University, Lanzhou 730000, China

⁴School of Science, Tibet University, Lhasa 850011, China

Correspondence: Taigang Zhang (zhangtg16@lzu.edu.cn) and Weicai Wang (weicaiwang@itpcas.ac.cn)

Abstract. The formation and expansion of glacial lakes worldwide due to global warming and glacier retreat have been well documented in the past few decades. Thousands of glacial lake outburst floods (GLOFs) originating from moraine-dammed and ice-dammed lakes were reported, causing devastating impacts on downstream lives and properties. Detailed glacial lake bathymetry surveys are essential for accurate GLOF simulation and risk assessment. However, these bathymetry surveys are still scarce as glacial lakes located in remote and high-altitude environments hamper a comprehensive investigation. We developed a conceptual model for glacial lake bathymetric distribution using a semi-automatic simulation procedure. The basic idea is that the statistical glacial lake volume-area curves conform to a power-law relationship indicating that the idealized geometric shape of the glacial lake basin should be hemispheres or cones. First, by reviewing the evolution of various types of glacial lakes, we identified 9 standard conceptual models to describe the shape of lake basins. Second, we defined a general conceptual model to depict the continuum transitions between different standard conceptual models for those specific glacial lakes that lie between two standard conceptual models. Third, we nested the optimal conceptual model into the actual glacial lake basin to construct the water depth contours and interpolate the glacial lake bathymetric distribution. We applied the conceptual model to simulate six typical glacial lakes in the Third Pole with in-situ bathymetric surveys to verify the algorithm's applicability. The results show a high consistency in the point-to-point comparisons of the measured and simulated water depths with a total volume difference of approximately $\pm 10\%$. The conceptual model has significant implications for understanding glacial lake evolution and modeling GLOFs in the future.

29 **1 Introduction**

30 Globally, glacial recession and thinning have been well-documented over the last decades via field observations
31 and remote sensing techniques (Yao et al., 2012; Zemp et al., 2019; Hugonnet et al., 2021). Such evolution of glaciers
32 due to climate warming and anthropogenic factors could induce related effects (Yao et al., 2019), among which is the
33 expansion and formation of glacial lakes (Zhang et al., 2015; Emmer et al., 2016; Wang et al., 2020; Ma et al., 2021).
34 Glacial lakes are water bodies developed within depressions of glacier moraine or mainly fed by contemporary glacier
35 meltwater (Yao et al., 2018). Due to glacier retreats, they are generally impounded by glacier terminal or lateral
36 moraine. Since the 1990s, the glacial lakes within 1 km buffer of the contemporary glaciers worldwide have increased
37 by around 50% in total number, area, and volume (Shugar et al., 2020). These changes have also been accompanied
38 by glacial lake outburst flood (GLOF) risks.

39 As a glacier-related hazard, GLOF has been a frequent incidence in various glacierized areas, causing
40 considerable socioeconomic losses (Anaconda et al., 2015a; Nie et al., 2018; Emmer et al., 2022a). According to a
41 compilation, more than 3,000 GLOFs from moraine- and ice-dammed lakes are recorded worldwide and claim more
42 than 10,000 deaths (Carrivick and Tweed, 2016; Lützow et al., 2023). Under the triggering factors such as ice
43 avalanches, landslides, and heavy precipitation, glacial lakes are extremely unstable and subsequently cause a sudden
44 release of water with peak discharge higher than a dozen times that of monsoon rainfall floods (Richardson and
45 Reynolds, 2000; Westoby et al., 2014; Kougkoulos et al., 2018). However, due to the relatively small volume of the
46 glacial lake, the flooding process generally attenuates rapidly within a few hours. Knowledge of glacial lake volume
47 is critical, as it influences the released water volume and GLOFs magnitude (Fujita et al., 2013). Therefore, lake
48 volume is often employed as an essential criterion in numerous cases of GLOF susceptibility and risk assessment
49 (Bolch et al., 2011; Aggarwal et al., 2017; Drenkhan et al., 2019; Falatkova et al., 2019).

50 Currently, only sporadic bathymetric surveys on glacial lakes have been conducted worldwide. In Cordillera
51 Blanca, Peru, facing continuous threats by GLOFs (Lliboutry et al., 1977), more than 100 detailed bathymetric
52 surveys of glacial lakes have been carried out to better understand the regional GLOF risks (Muñoz et al., 2020).
53 Government agencies and research institutions have promoted these surveys. In the Third Pole region, the bathymetric
54 surveys are focused on the glacial lakes in the Himalayas (Sharma et al., 2018; Watson et al., 2018), where
55 approximately 60 bathymetric surveys of glacial lakes, such as the Cirenmaco, Jialongco, and Longbasaba Lake,
56 were conducted (Yao et al., 2012; Wang et al., 2018; Li et al., 2021). They measure the water depth with ultrasonic

57 devices onboard automatic uncrewed boats or manual hovercrafts.

58 Performing a universal investigation campaign of lake bathymetry is impractical for thousands of glacial lakes
59 in remote areas and high elevations. Instead, scholars typically utilize single total lake volume data rather than
60 bathymetric distribution in GLOF modeling (Anaconda et al., 2015b; Zhang et al., 2021). The lake volume is typically
61 estimated by empirical equation, e.g., direct volume–area equation (O'Connor et al., 2001; Huggel et al., 2002;
62 Loriaux and Casassa, 2013), or indirect area–mean depth/maximum depth/width equation (Wang et al., 2012), which
63 have considerable uncertainty. There is no doubt that the measured and/or interpolated glacial lake bathymetric
64 distribution have great merit that can precisely determine the maximum potential outburst volume of the glacial lake,
65 serving to further simulate the GLOF propagation and evaluate downstream exposures (Frey et al., 2018; Sattar et
66 al., 2021). Moreover, a bathymetry survey is also pivotal to understanding the interactions between the glaciers and
67 their terminating lakes (Zhang et al., 2023), as several studies have revealed that the proglacial lake bathymetric state
68 can dominate the glacier terminal melting and calving regimes (Watson et al., 2020; Sugiyama et al., 2021).

69 Can we obtain glacial lake bathymetric distributions through modeling rather than in situ investigations?
70 Previous studies have provided insights. Cook and Quincey (2015) preliminarily proposed that the same type of
71 glacial lakes may have their idealized geometric shapes, which depict the evolution of glacial lakes' volume–area (V–
72 A) relationship over time. For instance, the triangular cone is suitable to represent the idealized geometric shape of
73 ice-dammed lakes dammed by glaciers and formed in the narrow valley. The idealized conceptual models of glacial
74 lakes can be combined with the actual situations to project the glacial lake bathymetric distribution.

75 An idealized lake basin is also helpful in constructing numerical or physical models. In the study of Veh et al.
76 (2020), the conceptual model of glacial lakes was constructed as a semi-ellipsoid with a circular surface to calculate
77 the released volume after the lake drainage. The surface area and height of the semi-ellipsoid refer to the glacier lake
78 area and maximum water depth, respectively. Based on these instructive designs, we attempted to develop a procedure
79 and algorithm for modeling glacial lake bathymetric distribution in this study. We first (i) retrieved as many as
80 possible conceptual models for various types of glacial lakes by reviewing the evolutions of glacial lakes and
81 analyzing the relationships between lake volumes and areas; (ii) explored the procedure and algorithm to estimate
82 bathymetric distribution in conjunction with actual lake surface and basin shapes; and then (iii) discussed their
83 implications and potential applications.

84 **2 Data and methods**

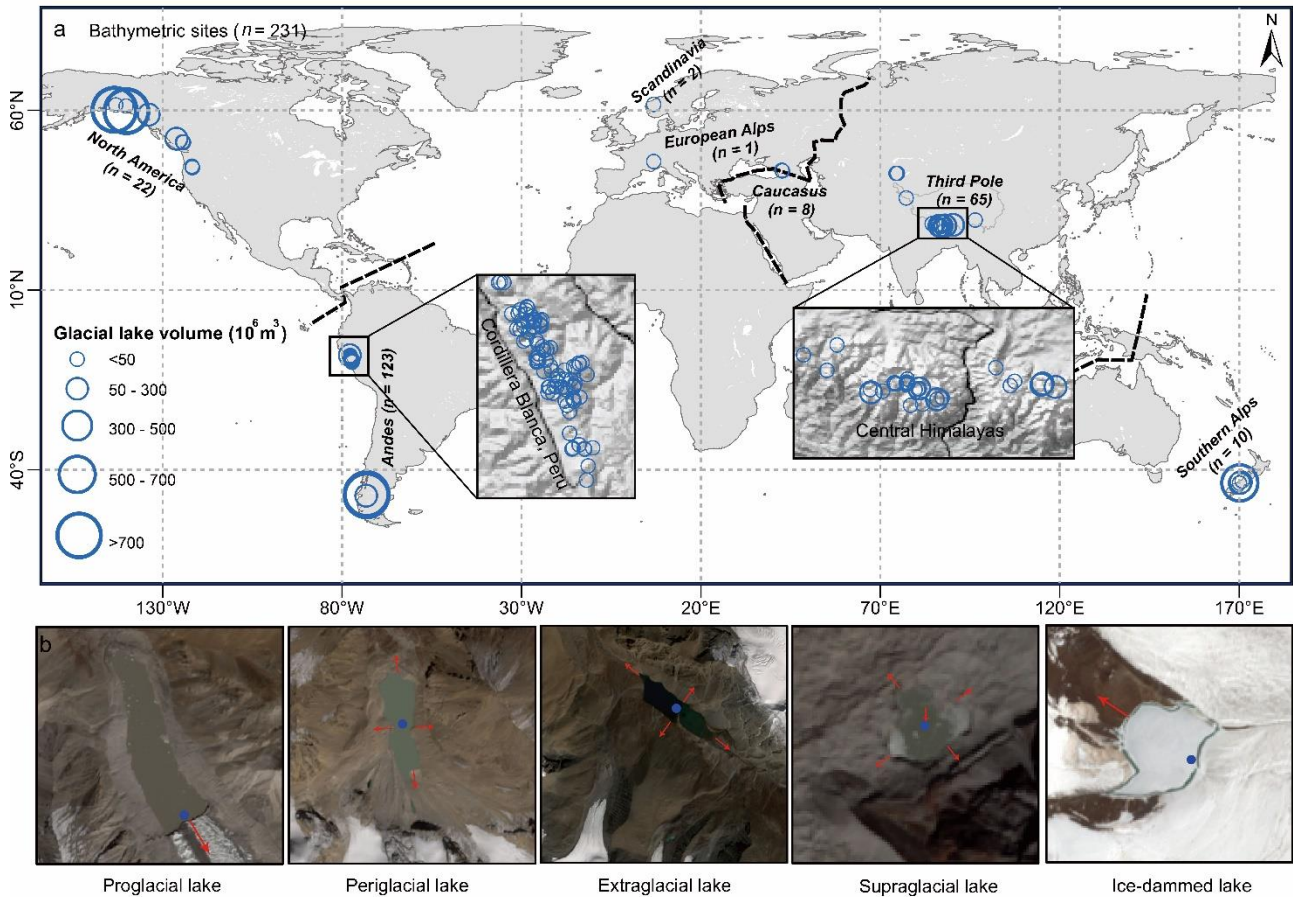
85 2.1 Compilation of glacial lake bathymetry

86 Analyzing the existing glacial lake bathymetries can help us reveal glacial lake water depth characteristics. To
87 our knowledge, more than 60 articles have mentioned surveyed bathymetry data from glacial lakes. We integrated
88 the prior studies and established an inventory of global glacial lake bathymetry (Supplementary material 1). The
89 attributes included the name, location, survey time, area, volume, and maximum water depth. A total of 231
90 bathymetric data from 220 glacial lakes globally were compiled in the inventory (Fig. 1a). Some large glacial lakes
91 were eliminated since their area deviate from the majority of concentration zone which could reduce the fitting
92 accuracy (Cook and Quincey, 2015).

93 2.2 Classification and evolution of different glacial lake types

94 The maximum water depth (D) and total volume (V) are the fundamental parameters regarding the idealized
95 geometric shape of glacial lakes. We used the compiled glacial lake bathymetry data to fit the curves of V–A (glacial
96 lake area) and D–A to understand the potential shapes of an idealized lake basin. Based on the topological positions
97 between the glacial lakes and their parent glaciers, we classified glacial lakes as proglacial, periglacial, extraglacial,
98 supraglacial, and ice-dammed types (Fig. 1b). This classification system considers glaciers' critical role in the
99 evolution of glacial lakes (Petrov et al., 2017; Rick et al., 2022).

100 We assumed that different types of glacial lakes have different expansion mechanisms and, thus, different
101 conceptual models (Carrivick and Tweed, 2013; Mertes et al., 2017; Minowa et al., 2023). The proglacial lake's
102 expansion mainly proceeds backward by glacial retreat (Minowa et al., 2023). For instance, Longbasaba Lake, located
103 in the central Himalayas, has substantially increased its surface area by occupying space liberated through glacier
104 terminal retreat since 1988, with limited expansion in the frontal and lateral moraine areas (Wei et al., 20201). The
105 periglacial lake and the extraglacial lake are not directly in contact with the glacier, and their expansion depends more
106 on changes in precipitation and glacier meltwater, thereby potentially expanding in all horizontal directions. As for
107 the supraglacial lake, expansion proceeds in all directions, and the temperature difference at the ice-water interface
108 continuously melts the glacier ice in both horizontal and vertical orientations (Watson et al., 2018). While for ice-
109 dammed lake, the evolution often appears horizontally with glacier retreat, as seen in the expansion of Merzbacher
110 Lake in the Tianshan Mountains (Gu et al., 2023). These various mechanisms in glacial lake expansions showed that
111 the changes in the lake basin among the different glacial lake types are inconsistent, indicating that they may have
112 different conceptual models.



113

114

115

116

117

118

119

120

121

Figure 1. (a) Distribution of glacial lakes whose volume was surveyed in detail. (b) Glacial lakes were divided into five categories, namely proglacial (direct in contact with glacier terminus), periglacial (separated from the glacier and dammed by historical moraine), extraglacial (far from the glacier and generally dammed by landslides), supraglacial (positioned on the glacier surface), and ice-dammed lake (formed when glacier surges block downstream valleys or meltwater fills depressions between retreating tributary and main glaciers). Red arrows indicate the possible main directions of expansion of the glacial lake, and the blue points represent the location of maximum water depth. [The Sentinel-2 images were selected to exhibit these glacial lakes.](#)

2.3 Standard conceptual model

122

123

124

125

126

The basic procedure of constructing glacial lake bathymetric distribution is to (i) identify the most appropriate conceptual model that can describe the idealized lake basin, (ii) calculate the theoretical formulation equations of this conceptual model, (iii) nest this conceptual model into the actual glacial lake basin to construct the water depth contours, and (iv) interpolate and calculate the glacial lake bathymetric distribution. The conceptual model was constructed as the scheme presented by Veh et al. (2020). Glacial lakes were assumed to have hemispherical or similar

127 three-dimensional lake basin shapes. The standard surface of the glacial lake was assumed to be an ellipse.

128 The general formula between the volume and area of glacial lakes fits a power-law relationship (Table 1). It
129 could be expressed as Eq. (1). The best-fit curve for the relationship between maximum water depth and area of
130 glacial lakes also follows the power-law relationship (Eq. 2) (Fig. 2).

$$131 \quad V = \alpha A^\beta \quad (1)$$

$$132 \quad D = \gamma A^\varepsilon \quad (2)$$

133 A is the area of the glacial lake; α , β , γ , and ε are the coefficients. The value of β is greater than 1, and ε
134 is less than 1.

135 The three-dimensional bodies representing the standard shape of a lake basin were required to have a general
136 formula as defined by Eq. (3):

$$137 \quad V = \delta AD \quad (3)$$

138 Here, δ is the coefficient, A is the elliptical surface area, and D corresponds to the maximum water depth of
139 the glacial lake. We identified four hemispheres or cones whose volumes can be expressed by Eq. (3): the hemisphere
140 structured by the elliptical side ($V = 2/3AD$); the hemisphere structured by the upward-opening parabolic side ($V =$
141 $1/2AD$); the cone structured by the straight side ($V = 1/3AD$); and the cone structured by the rightward-opening
142 parabolic side ($V = 1/5AD$). These bodies are defined as the standard conceptual model (SCM), and their curves in
143 the X-O-Z quadrant are called the standard curves (Fig. 3a). These four standard curves are progressively concave
144 inward in the quadrant, from the elliptical curve to the rightward-opening parabolic curve.

145 These SCMs for the supraglacial, periglacial, and extraglacial lakes are compatible with the expansion
146 mechanisms partly because their growth direction is comprehensive at the horizontal level. Their maximum water
147 depths were set in the lake center. However, proglacial and ice-dammed lakes are different. Their expansions are
148 focused toward the glacier's or valley's direction, and the maximum water depths are generally situated near the
149 intersection with the glacier, [\(e.g. Longbasaba proglacial lake \(Yao et al., 2012; Wei et al., 2021\); and Shisper ice-](#)
150 [dammed lake \(Singh et al., 2023; Gu et al., 2023\)](#). Under these circumstances, we considered the SCMs of proglacial
151 lakes to be half of the preceding four SCMs, namely the semi-hemisphere structured by the elliptical side ($V = 1/3AD$);
152 the semi-hemisphere structured by the upward-opening parabolic side ($V = 1/4AD$); semi-cone structured by the
153 straight side ($V = 1/6AD$); and the semi-cone structured by the rightward-opening parabolic side ($V = 1/10AD$). We

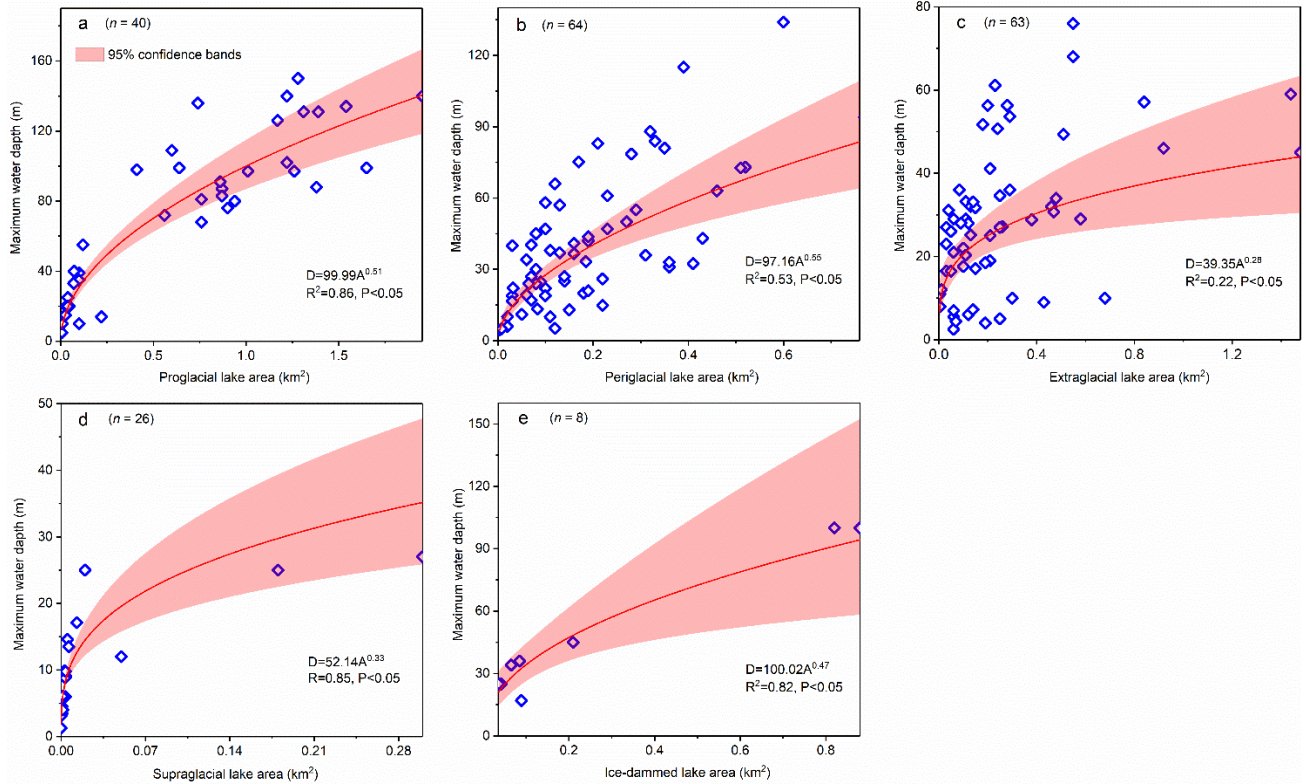
154 designed two SCMs for the ice-dammed lake (Fig. 3a): the semi-cone structured by the straight side ($V = 1/6AD$) and
 155 the triangular cone ($V = 1/3AD$). The deepest point for proglacial and ice-dammed lake were set near the glacier-lake
 156 interface. Most of the actual volume points lie between the volume curves of these SCMs (Fig. 4), and there are one
 157 or two closer SCM volume curves for each type of glacial lake's fitted A–V curve. Ultimately, a total of 9 different
 158 SCMs were designed to express the idealized geometric shapes of glacial lake basin.

159

160 **Table 1.** Empirical equations of volume and area of glacial lakes in previous studies. The applicable region, lake type, and sample size
 161 for each empirical equation were indicated during fitting. The volume unit is 10^6 m^3 , and the area unit is km^2 . In the dam material-
 162 based classification method for glacial lakes, a substantial number of proglacial and periglacial lakes can be categorized as moraine-
 163 dammed lakes.

ID	Empirical formulas	Region	Lake types	Samples	Reference
1	$V = 35A^{1.5}$	British Columbia, Canada	Ice-dammed lake	not mentioned	Evans, 1986
2	$V = 168.5A^2 + 3.11A$	Northwestern America	Moraine-dammed lake	7	O'Connor et al., 2001
3	$V = 34.44A^{1.42}$	Worldwide	Moraine- and ice-dammed lake	13	Huggel et al., 2002
4	$V = 43.24A^{1.53}$	Himalayas	Moraine-dammed lake	17	Sakai, 2012
5	$V = 6.07A^{1.37}$	Himalayas	Moraine-dammed lake	20	Wang et al., 2012
6	$V = 55A^{1.25}$	Himalayas	Moraine-dammed lake	20	Fujita et al., 2013
7	$V = 33.58A^{1.39}$	Worldwide	Moraine- and ice-dammed lake	31	Loriaux and Casassa, 2013
8	$V = 42.93A^{1.48}$	Peruvian Andes	Moraine- and bedrock-dammed lake	35	Emmer and Vilímek, 2014
9	$V = 34.07A^{1.37}$	Worldwide	Various types	69	Cook and Quincey, 2015
10	$V = 11.49A^{1.26}$	Worldwide	Supraglacial lake	9	Cook and Quincey, 2015
11	$V = 60A - 6.28$	Worldwide	Moraine-dammed lake	42	Cook and Quincey, 2015
12	$V = 2.63e^A$	Worldwide	Ice-dammed lake	9	Cook and Quincey, 2015
13	$V = 37.3A^{1.47}$	Himalayas	Moraine-dammed lake	33	Khanal et al., 2015
14	$V = 52.2A^{1.18}$	Himalayas	Proglacial lake	6	Sharma et al., 2018
15	$V = 40A^2 + 5.06A$	Himalayas	Moraine-dammed lake	17	Patel et al., 2017
16	$V = 35.36A^{1.47}$	Central Asia	Moraine-dammed lake	32	Kapitsa et al., 2017
17	$V = 32.13A^{1.49}$	Himalayas	Ice-dammed lake, supraglacial lake	not mentioned	Miles et al., 2018
18	$V = 28.95A^{1.33}$	Worldwide	Moraine-dammed lake	93	Watson et al., 2018
19	$V = 35.46A^{1.4016}$	Himalayas	Supraglacial lake	24	Watson et al., 2018
19	$V = 41WA + 2A$	Cordillera Blanca, Peru	Moraine-dammed lake	120	Muñoz et al., 2020
20	$V = 37.36A^{1.41}$	Peruvian Andes	Various types	170	Wood et al., 2021
21	$V = 38.04A^{1.36}$	Peruvian Andes	Moraine-dammed lake	not mentioned	Wood et al., 2021
22	$V = 43.27A^{1.64}$	Peruvian Andes	Unclassified	not mentioned	Wood et al., 2021

164

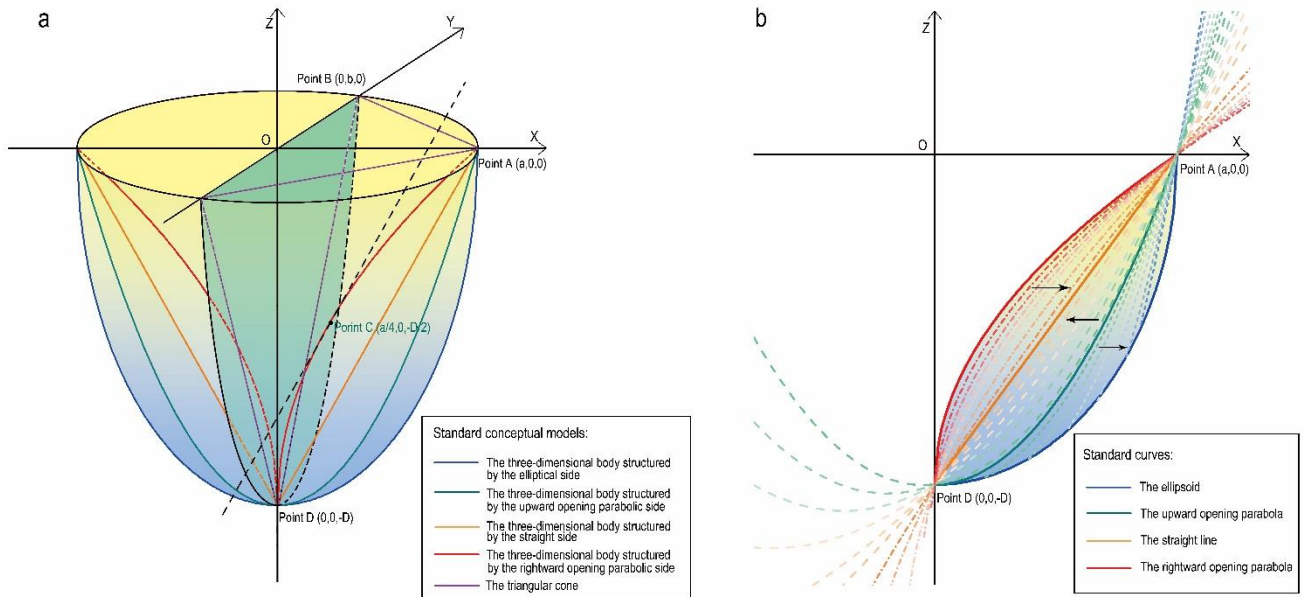


165

166

167

Figure 2. Relationships between maximum water depth and the area of glacial lakes were compiled in the present study for the following lake types: (a) proglacial lake, (b) periglacial lake, (c) extraglacial lake, (d) supraglacial lake, and (e) ice-dammed lake.



168

169

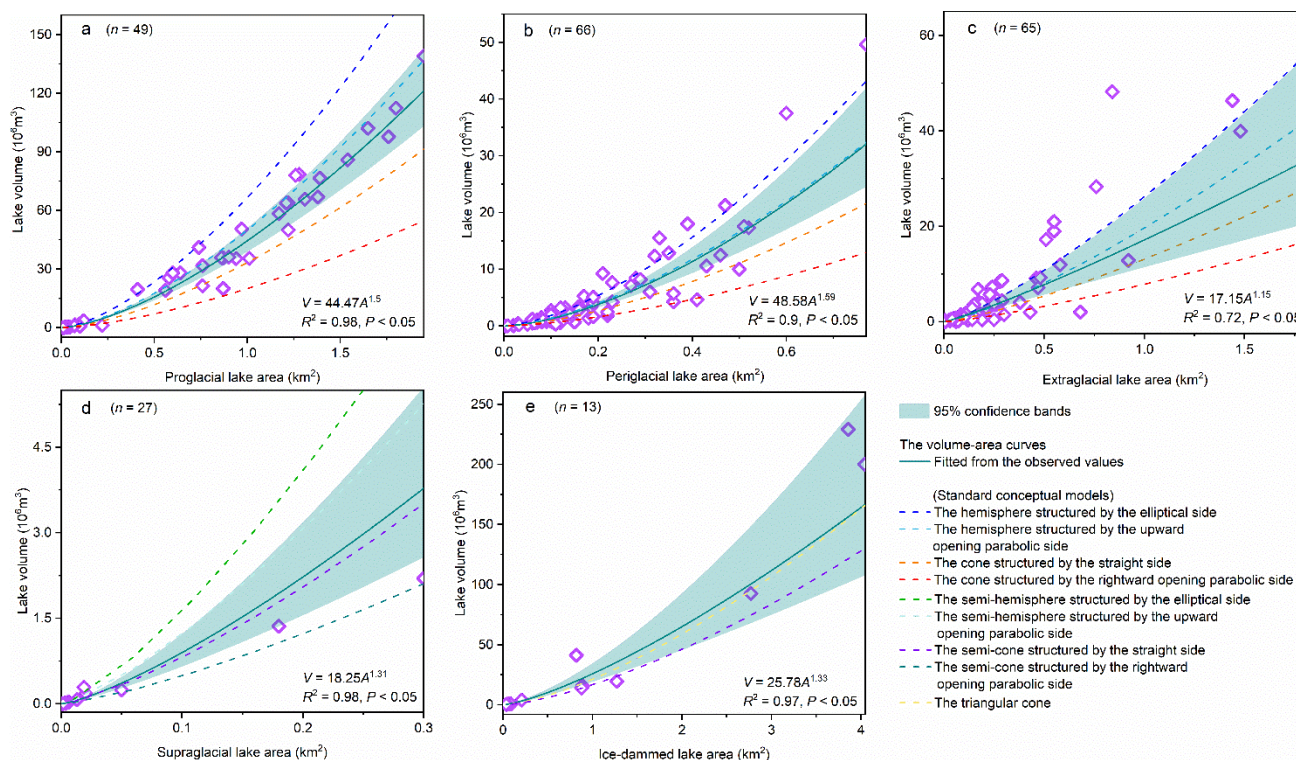
170

171

172

Figure 3. (a) Schematic diagram illustrates the shapes of the SCMs, namely the hemisphere structured by the elliptical side/upward-opening parabolic side, the cone structured by the straight side/rightward-opening parabolic side, the triangular cone, as well as their shapes when symmetrically divided matching the SCMs of the proglacial lake. Here, A is the semi-long axis, B is the elliptical surface's semi-short axis, and D is the maximum water depth. (b) Convergences of the general curves towards the standard curves in the X–O–Z

173 quadrant in different orientations.



174

175 **Figure 4.** Relationships between the volume (V) and area (A) of glacial lakes were compiled in the present study for the following lake
 176 types: (a) proglacial lake, (b) periglacial lake, (c) extraglacial lake, (d) supraglacial lake, and (e) ice-dammed lake. The dotted lines
 177 indicate the volume curves of different standard conceptual models, which were fitted by Eq. (2) and (3).

178 2.4 General conceptual model

179 If a specific glacial lake has determined its parameters such as surface size, maximum water depth, and volume,
 180 it is unlikely that the closest SCM would accurately represent the most appropriate conceptual model. This is because
 181 the relatively inherent volume of the SCM is hardly equal to the volume of a specific glacial lake. In other word, the
 182 volume curve of the SCM is constant, and therefore, the volume point of a specific glacial lake may deviate from the
 183 SCM volume curve. Consequently, directly using the SCM to nest and interpolate a realistic glacial lake bathymetric
 184 distribution would result in an initial over- or underestimation of the total lake volume.

185 The SCMs can only help us comprehend the various glacial lake morphologies; they cannot be applied directly
 186 to estimate the glacial lake bathymetric distribution. We may conceive the measured volume points between the SCM
 187 volume curves as a result of the transition from one SCM to another. For instance, from the upward-opening parabolic
 188 line to the straight line, it is the standard parabolic line continuously approximating the straight line on the X-O-Z

189 quadrant by moving downward and left (Fig. 3b). During the movement process, the rotated-out hemisphere is
190 moving toward the cone structured by the straight side. We can capture these general conceptual models (GCMs) in
191 this transition stage and make their volume consistent with the measured or estimated lake volume. This means we
192 find a GCM that is more effective than the SCM in estimating the lake depth distribution.

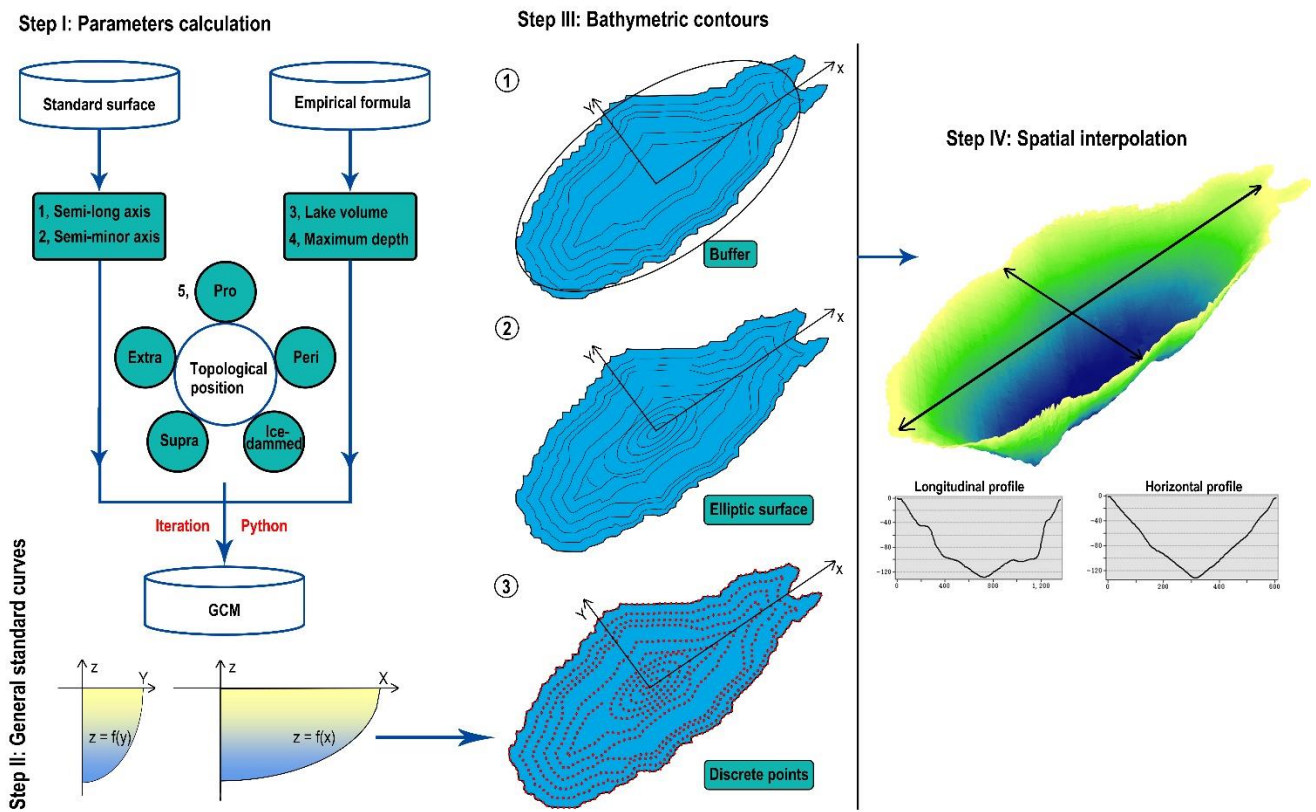
193 Python programming was used to drive the standard curves' transition and parameter calculations. The
194 theoretical description for the GCMs is presented in supplementary material 2. By relocating the standard curve's
195 vertices and altering the opening size, it is simple to compute the transition of a standard upward/rightward-opening
196 parabola to a straight line. The resultant general curves must pass through points A and D. The convergence to the
197 standard elliptic curve from the standard upward-opening parabola is relatively complicated. If we move the vertices
198 of the standard parabola to the right and downward, the maximum height of the produced GCM changes. We used a
199 compound style here. When the second intersection of the moved general parabolic curve and the standard elliptic
200 curve occurs (from right to left), the side of GCM starts to take the elliptic curve change. Additionally, the marginal
201 SCMs should be employed when the measured volume is larger (smaller) than the largest (smallest) SCM volume.

202 **2.5 Nesting the actual glacial lake shapes**

203 Once a given glacial lake's GCM has been established, the lake's bathymetric contours may be predicted in
204 relation to actual conditions and parameters. Since the actual shape of the glacial lake surface is irregular, rather than
205 the normal elliptic surface we used in the models, it was crucial to determine how the depth contours move inward
206 based on the actual shape.

207 We tested two hypotheses. First, utilizing the lakeshore line to continually create buffers inward might depict
208 the depth contours because the depth contours near the lakeshore were the consequence of ongoing indentation of the
209 actual glacial lake surface outline inward. Second, at the 1/4 semi-long axis of the standard elliptic surface, the depth
210 contours would become progressively blurred as the inward indentation continues, thus subsequently using the
211 standard elliptic surface to start the inward indentation (Fig. 5). Importantly, these assumptions were supported by
212 observations of hundreds of glacial lake bathymetric distribution cases worldwide. Some similarities exist between
213 the bathymetric contours and the lakeshore shape, suggesting that the area near the lakeshore is possibly impacted by
214 the slopes around the lake and/or other material sources. There are two explanations for this phenomenon: either the
215 glacial lakes were continuously filled with exogenous debris and rocks, or the initial lake water level had risen and
216 flooded part of the original slopes.

217 The 1/4 semi-long axis is the ending position where the glacial lake is not impacted by exogenous materials, as
 218 determined by our understanding of those SCMs. Most of the glacial lake SCMs were located closer to the cone,
 219 structured by the straight side of the hemisphere and the upward-opening parabolic side. It is inferred that the initial
 220 deepening of the glacial lake is not particularly large from the outer line to the center (compared to the semi-ellipsoid),
 221 indicating that exogenous materials are likely to have impacted it. This situation is better understood when the lake
 222 SCM is a cone structured by the rightward-opening parabolic side. Therefore, we hypothesized an extreme
 223 circumstance in which a glacial lake starts to be significantly influenced by the lake's surroundings' topography. In
 224 this case, the slope of the standard rightward-opening parabolic curve is smaller than the slope of the standard straight
 225 line and closer to the ideal deepening state of the lake basin when it is larger. This equal slope point is located at the
 226 1/4 semi-long axis and represents half of the maximum water depth.



227
 228 **Figure 5.** The procedure illustrates the parameter calculation of GCMs and processes of creating buffers inward. The water depths on
 229 the axes were calculated using the standard curves corresponding to the X and Y axes.

230 **2.6 Sites for exhibiting and validating results**

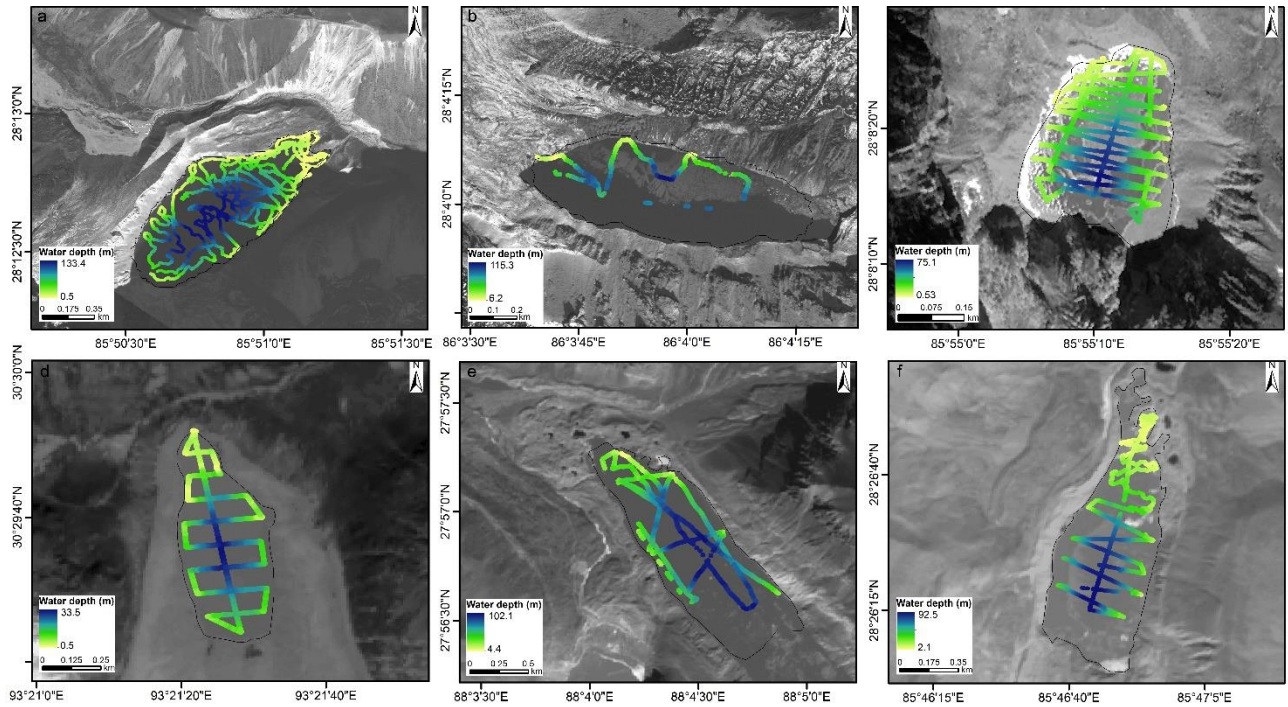
231 Six sets of bathymetry data were collected for the typical glacial lakes in the Himalayas and Nyainqentanglha
 232 (Fig. 6). Among them, Jialongco, Cirenmaco, Poiqu NO.1, and Maqiongco were classified as periglacial lakes, while

233 the Longbasaba Lake and Dasuopuco were classified as proglacial lakes. Although it would be desirable to evaluate
 234 the performance of our conceptual models across different types, sizes, and geographic locations of glacial lakes, we
 235 were limited by the available observational data and could only conduct these examinations in the Third Pole region,
 236 focusing on proglacial and periglacial lake types. The topological position, total volume, maximum water depth, and
 237 semi-long/minor axis of the standard lake surface were crucial parameters in glacial lake bathymetric distribution
 238 modeling (Table 2). The six glacial lake bathymetric distributions were simulated according to the lake sizes in the
 239 survey year and eventually compared with the measured points of water depths and the overall parameters (total
 240 volume and mean water depth) to verify the feasibility and accuracy of our modeling method.

241 **Table 2.** The crucial modeling parameters of the six selected glacial lakes.

Name	Lat°	Lon°	Region	Topological position	Survey year	Area (km ²)	Volume (10 ⁶ m ³)	Mean water depth (m)	Maximum water depth (m)	Semi-long axis (m)	Semi-minor axis (m)
Jialongco	28.21	85.85	Central Himalaya	periglacial	2020	0.61	37.5	58.2	133	757	314
Cirenmaco	28.07	86.07	Central Himalaya	periglacial	2012	0.33	18.0	55	115	549	185
Poiqu NO.1	28.14	85.92	Central Himalaya	periglacial	2021	0.11	2.7	25.5	75.1	242	129
Maqiongco	30.49	93.36	Nyainqentanglha	periglacial	2021	0.23	3.2	15	33.5	493	168
Longbasaba Lake	27.95	88.08	Eastern Himalaya	proglacial	2009	1.17	64.0	48	102	1949	319
Dasuopuco	28.44	85.78	Central Himalaya	proglacial	2021	0.55	0.55	33.8	93	1362	247

242



243

244 **Figure 6.** The water depth observed along the bathymetric routes for (a) Jialongco, (b) Cirenmaco, (c) Poiqu NO.1, (d) Maqiongco, (e)

245 Longbasaba Lake, and (f) Dasuopuco.

246

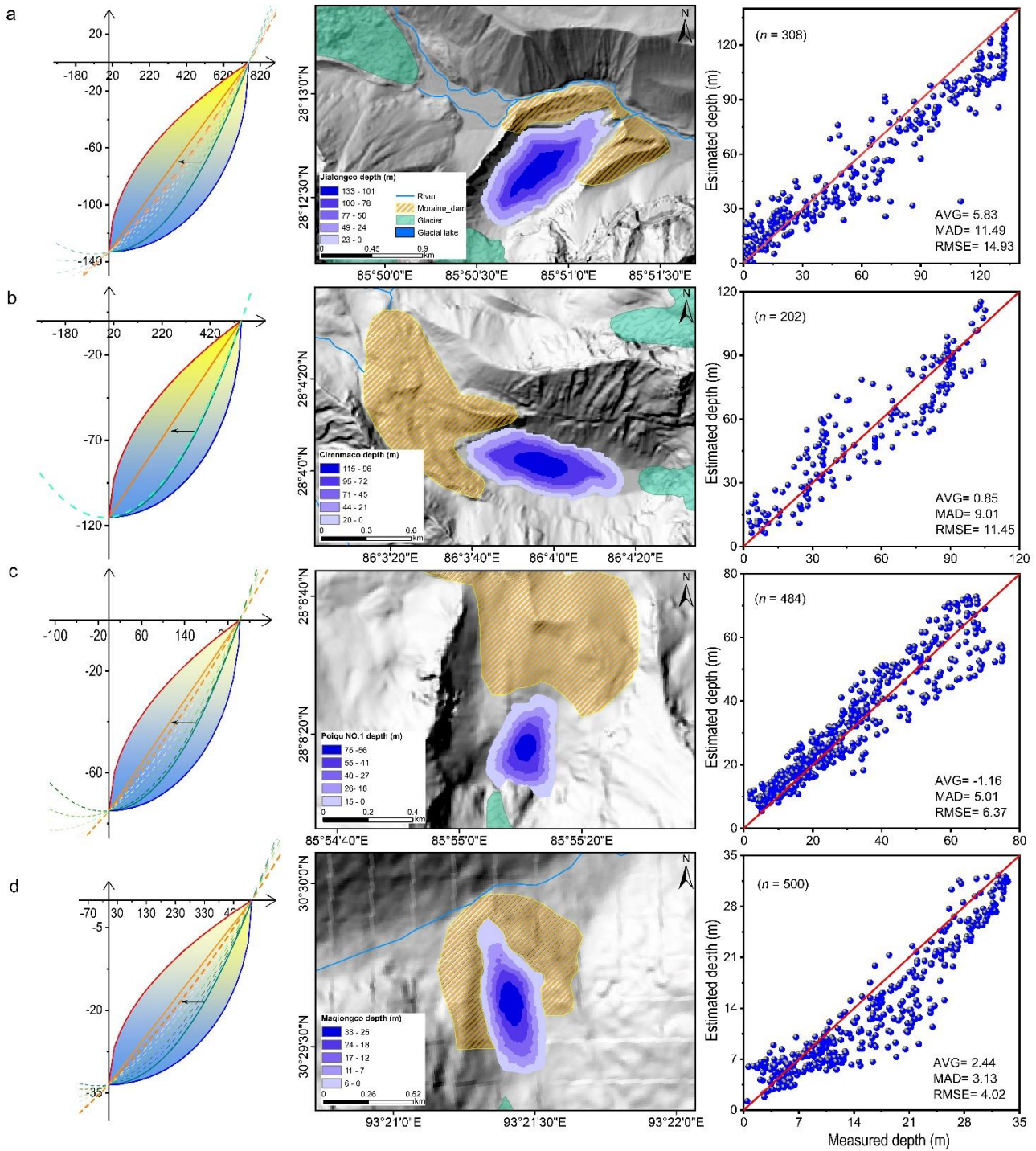
247 **3 Results**

248 We present the SCMs for each type of glacial lake and demonstrate a procedure to identify the most compatible
249 GCM for a specific glacial lake by equalizing the volume of both. To our knowledge, this is the first model to simulate
250 the bathymetric distribution of glacial lakes at present. The results reveal that the proglacial and periglacial lakes
251 exhibit greater depths as their SCMs are closer to the hemisphere structured by the upward-opening parabolic side.
252 Conversely, the SCMs of the extraglacial and supraglacial lakes are closer to the cone structured by the straight side,
253 indicating relatively shallower depths. As the ice-dammed lake, their V–A fitting curve is more similar to the V–A
254 curve of the triangular cone (Fig. 4). Hence, we recommend that the bathymetric distribution modeling for ice-
255 dammed lakes proceeds directly using the standard triangular cone.

256 We determined the optimal GCMs for the six exhibited glacial lakes. Following bathymetric distribution
257 modeling results, the total volume of Jialongco was calculated to be $33.1 \times 10^6 \text{ m}^3$ (with a relative error of -11.7%)
258 with a mean water depth of 54.6 m (-8.1%). Its GCM was closer to the cone structured by the straight side (Fig. 7a).
259 The computed total volume and mean depth of Cirenmaco were $17.2 \times 10^6 \text{ m}^3$ (-4.4%) and 51.7 m (-6.9%),
260 respectively. The Cirenmaco GCM had similarities with the hemisphere structured by the upward-opening parabolic
261 side (Fig. 7b), meaning a more significant inward deepening rate than Jialongco. The relatively small-sized Poiqu
262 NO.1 and Maqiongco had total volumes of $2.9 \times 10^6 \text{ m}^3$ (7.4%) and $3 \times 10^6 \text{ m}^3$ (-6.3%), and mean water depths of 27.3
263 m (7.1%) and 12.8 m (-14.7%), respectively. Their optimal GCMs showed similarities with Jialongco (Fig. 7c,
264 d). The proglacial lake, Longbasaba, was estimated to have a total volume of $71.4 \times 10^6 \text{ m}^3$ (11.5%) and a mean depth
265 of 61.1 m (22.2%). Its GCM was more resemblant to the semi-ellipsoid (Fig. 8a). Dasuopuco had the smallest relative
266 error in the total volume (0.2%) and mean water depth (-1.8%) (Fig. 8b). Overall, approximately $\pm 10\%$ volume
267 uncertainty was estimated in the process of nesting the general conceptual models to the actual glacial lake shapes.

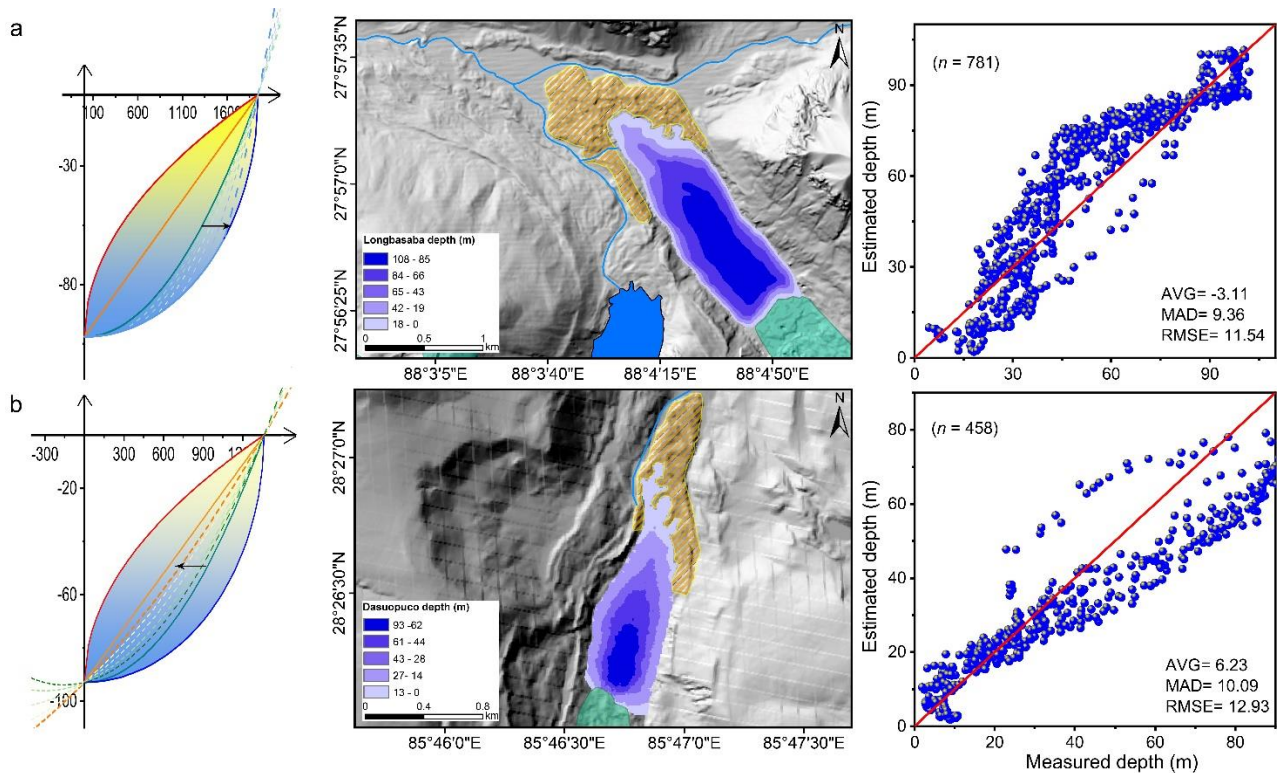
268 The disparity between the area of the assumed standard ellipse surface and the actual lake surface, as well as the
269 deviation of the deepest water location, likely caused the majority of the inaccuracy. The initial settings of glacial
270 lake conceptual models and the algorithm's applicability were confirmed by comparison with the measured and
271 estimated individual water depths. Between the estimated and measured water depths along the bathymetric routes,
272 the average deviation, mean absolute deviation, and root mean square error for the six glacial lakes all described good

273 consistency. Neither near the lakeshore nor the lake center do the estimates show intolerable dispersions.



274

275 **Figure 7.** Modeled glacial lake bathymetric distributions of the four selected periglacial lakes. (a) Jialongco, (b) Cirenmaco, (c) Poiqu
 276 NO.1, and (d) Maqiongco. The average deviation (AVG), mean absolute deviation (MAD), and root mean square error (RMSE) were
 277 selected to depict the consistency between the simulated and measured individual water depths along the boat routes. The movements
 278 of the general curves from one standard curve to another are also indicated.



279

280 **Figure 8.** Modeled glacial lake bathymetric distributions of the two selected proglacial lakes. (a) Longbasaba Lake, and (b) Dasuopuco.
 281 The average deviation (AVG), mean absolute deviation (MAD), and root mean square error (RMSE) were selected to depict the
 282 consistency between the simulated and measured individual water depths along the boat routes. The movements of the general curves
 283 from one standard curve to another are also indicated.

284

285 4 Discussion

286 4.1 Glacial lake basin evolution

287 Understanding the glacial lake evolution can help comprehend these idealized geometric shapes in theory. Most
 288 moraine- or bedrock-dammed lakes develop in depressions exposed by diminishing glaciers. The supraglacial lakes
 289 exist at the glacier snout, eventually facilitating the formation of proglacial and periglacial lakes (Carrivick and Tweed,
 290 2013; [Mertes et al., 2017](#)). As the six glacial lakes illustrated, our hypotheses explained the different rates of inward
 291 deepening owing to the influence of exogenous materials. The glacier bedrock has been eroded and nudged during
 292 historical ice flowing, posing the excavation and growth of glacial lake basins.

293 Contemporary glaciers often have a certain thickness of debris at the snout. For example, approximately 1 m of
 294 debris was observed at the snout of the Urumqi Glacier No. 1, China (Echelmeyer et al., 1987) as the result of glacial

295 erosion. The specific sites of continual eroding and nudging spawn overdeepenings and are considered potential
296 glacial lakes (Linsbauer et al., 2016). Since the glacier velocity in the middle part is often larger than that of both
297 sides, the erosion is stronger in the central line of the initial overdeepening. As glacier flowing continues, the shape
298 of the overdeepening finally reaches equilibrium and is similar to a hemisphere, which is the GCM of the lake basin
299 we assumed. After the overdeepenings are exposed, they can be filled by meltwater to form glacial lakes while also
300 receiving material deposition, resulting in a gradual transition of the idealized geometric basin from a hemisphere to
301 a cone. This conjecture can be inferred from the studies of overdeepenings on glacial beds, whereby the volume and
302 surface area of these potential glacial lakes are also in accordance with the power-law relationship (Zhang et al.,
303 2022).

304 4.2 Applicability of the conceptual model

305 Our modeling theory is based on the observations of glacial lake bathymetric distribution characteristics
306 worldwide, revealing a ~~universal~~ geometrical approximation law for glacial lake bathymetry. ~~Therefore, this~~
307 ~~modeling approach may be applicable to most glacial lakes in mountain glaciers.~~ However, it is strictly limited by
308 several constraints. Firstly, the designed conceptual model is more suitable for those glacial lakes with typically
309 lengthy and elliptical-like shapes, and may be less applicable to very irregularly shaped glacial lakes, such as the ice-
310 marginal and thermokarst lakes in the Greenland and Alaska region (Field et al., 2021; Coulombe et al., 2022).
311 ~~Similarly, we did not collected any glacial lake bathymetry data in polar regions which causes non-applicability on~~
312 ~~supraglacial lakes over the Greenland/Antarctic Ice sheets.~~ Secondly, the designed conceptual model is also more
313 suitable for those glacial lakes with the parent glaciers of glacial lakes can be a cirque-valley glacier or a
314 small/medium sized valley glacier flowing along a straight valley, ensuring idealized formation conditions for the
315 glacial lake basin with minimal erosion and deposition from tributaries. _

316 Although the simulated results were only validated in the periglacial and proglacial lakes of the Himalayas and
317 Nyainqentanglha due to limited observation data, the comparison results of the measured and modeled depth values
318 at different locations of the six glacial lakes demonstrates the rationality and reliability of our conceptual models.
319 Further validation is needed to assess the applicability of our conceptual model across different lake types on a global
320 scale. There is a significant limitation in the availability of glacial lake bathymetric distribution data, with most
321 studies only providing key parameters such as total volume, maximum depth, and mean depth. Moreover, due to the
322 challenges of field investigations, measurements of glacial lakes have predominantly focused on larger, hazardous,

323 or particularly interesting peri- and proglacial lakes. This makes us unable to find any available bathymetric
324 distribution data for extraglacial, supraglacial, and ice-dammed lakes, preventing validation of our conceptual model
325 for these lake types.

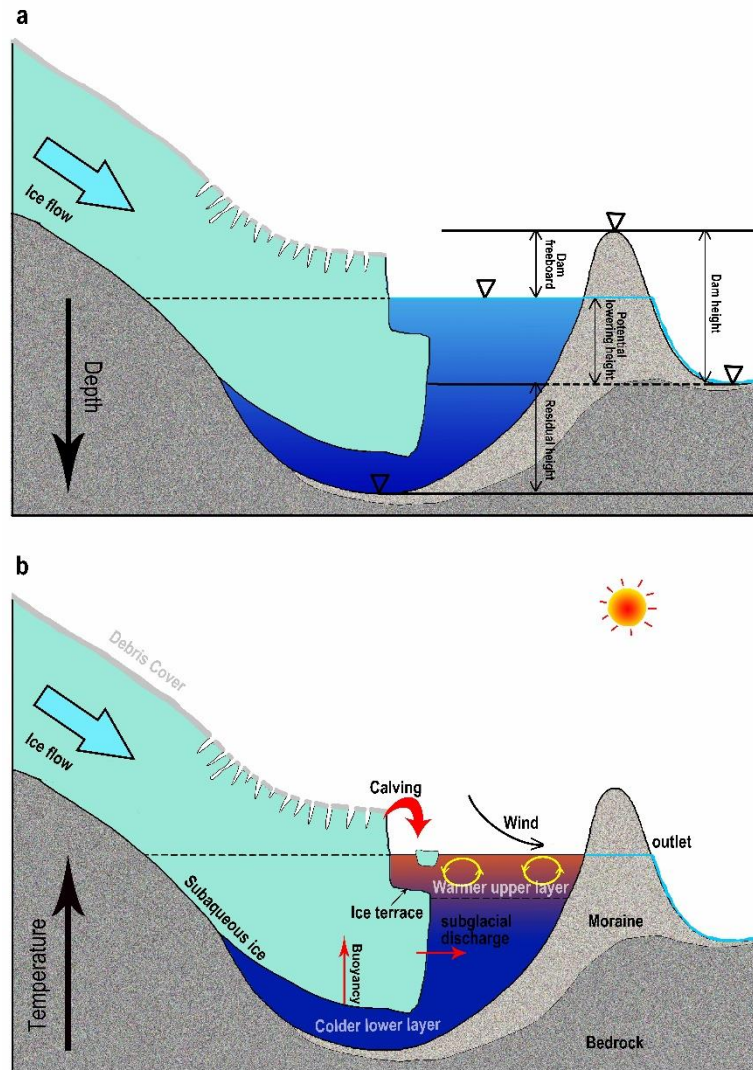
326 In addition to the subjective and objective errors made during the modeling phase, there are several systematic
327 defects in the algorithm itself: (1) The total volume and maximum water depth are calculated using empirical
328 equations, which may lead to significant deviations when modeling the bathymetric distribution of an arbitrarily
329 selected glacial lake. Particularly, the curves of D–A are not robust, with many discrete points appearing (Fig. 2). (2)
330 The estimated depth contours converge inward using the lake shoreline buffers first, followed by the elliptical
331 surfaces. This process may effectively simulate the connections between a bathymetric distribution and glacial lake
332 morphology. However, it is not essential. If the elliptical indentations are always inward relative to the elliptical
333 surface, the modeling accuracy is also not affected significantly in theory. (3) The deepest sites of proglacial lakes
334 have been considered to be near the glacier-lake interface. The developing proglacial lakes, however, are complex.
335 Their deepest sites are constantly located near the glacier terminus before the deepest site of overdeepening is exposed
336 (Fig. 9a), which is in accordance with our hypothesis. With the deepest sites developing more fully, they gradually
337 shift toward the lake center. Our algorithm has not addressed these changes. In the future, the conceptual model will
338 require parameter optimization through learning with a number of measured bathymetry data. Furthermore, the
339 present version of our algorithm relies on simple programming and semi-automated geospatial analysis tools
340 processing. We will further develop this conceptual model to create an interface that can automatically process and
341 reduce subjective errors.

342 **4.3 Rationality of empirical V-A equations**

343 Currently, many studies have attempted to fit V-A equations with regional or global applicability for various
344 types of glacial lakes (Cook et al., 2015; Qi et al., 2022). The most common classification method for glacial lakes is
345 based on dam materials, such as moraine-dammed, bedrock-dammed, and landslide-dammed. However, this study
346 reveals that the different types of glacial lakes have different ideal basin shapes that may be unfavorable to most
347 already formed V-A empirical formulations, although some have high R^2 values (Table 1). For instance, most of the
348 proglacial and periglacial lakes is generally dammed by moraine, involving in many fitting works of V-A relationships.
349 Unreasonably, the incompletely developed basins of proglacial lakes and the fully developed basins of periglacial
350 lakes are often described by same empirical formulas (Fig. 9a), disregarding the distinct basin development stages

351 between them. This aspect has overlooked in the previous studies. In our fitted curves of V-A relationships for various
352 types of glacial lakes (Fig. 4), the V-A relationship for proglacial lakes is robust, indicating possible global
353 applicability. However, the V-A relationships for periglacial and extraglacial lakes exhibit many outliers, suggesting
354 a strong influence from exogenous materials filling in these lakes based on our hypothesis. The V-A relationships of
355 these glacial lakes decoupled with their glaciers at least require parameters related to the glacier characteristics and
356 time of detachment for further description.

357 There is no single classification method can adequately capture the refined characteristics of glacial lakes. Even
358 lakes classified as the same type may differ in terms of parent glaciers, bedrock properties, or dam materials. In the
359 modeling of glacial lake bathymetric distribution, accurately estimating the total volume and maximum water depth
360 of glacial lakes is crucial. Therefore, future studies should not only focus on whether the empirical formula is
361 generalizability or global applicability, but also develop more detailed classification criteria for glacial lakes,
362 comprehensively considering dam materials, topological positions, glacier properties, area intervals, geographic
363 location, and other relevant factors. This will facilitate a well-fitting of regional empirical relationships of V-A and
364 D-A for various types of glacial lakes, thereby reducing the dispersion between data points.



365

366 **Figure 9.** The schematic diagrams illustrate (a) the potential maximum lowering height of the glacial lake water level after drainage and
 367 (b) the interactions between the parent glacier and its terminating lake.

368 **4.4 Applications in GLOF modeling**

369 The ~~applicability of a glacial lake bathymetric distribution conceptual model~~ has been ~~addressed~~ proposed in this
 370 study; one such application is in GLOF modeling. The results make two significant contributions to future GLOF
 371 modeling: (i) accurately estimate the maximum potential outburst water volume of a glacial lake by combining lake
 372 surface elevation, dam bottom elevation, and the optimal GCM; (ii) facilitate coupling between the various GLOF
 373 processes in modeling (trigger–displacement wave–dam breach–flood propagation). Many recent studies have
 374 documented reconstructing the historical GLOFs and simulating the future GLOFs from high outburst potential
 375 glacial lakes (Allen et al., 2015; Anaconda et al., 2015b; Erokhin et al., 2017; Kougkoulos et al., 2018). The modeling

376 precision is expected to improve significantly.

377 On the one hand, most prior studies replaced the potential maximum outburst volume with the total water volume
378 because of the limitations of glacial lake bathymetric investigations (Zhang et al., 2021). Although this could present
379 a maximized risk assessment, an inflated downstream exposure might raise excessive concerns among the authorities
380 and the public regarding inadequate prevention and mitigation measures (Emmer et al., 2022b). As long as the dam's
381 lowest elevation exceeds that of the glacial lake (potential lowering height is less than the maximum water depth), it
382 could result in incomplete drainage (Fig. 9a). On the other hand, due to the complicated phase transition in the chain
383 process of GLOFs, a segmented simulation has been generally conducted. For instance, Rapid Mass Movement
384 Simulation (RAMMS) can be used to simulate the impact of ice avalanches or landslides on glacial lakes (Frey et al.
385 2018; Sattar et al. 2021; [Duan et al., 2023](#)), and hydrological algorithms are used to calculate the displacement wave
386 (Heller et al. 2009; Evers et al. 2019). Modeling software like IBER, HEC-RAS, or FLO-2D are employed to simulate
387 downstream flood propagation (Alho and Aaltonen, 2008; Osti and Egashira, 2009; Schneider et al., 2014; Somos-
388 Valenzuela et al., 2015; Maurer et al., 2020; Nie et al. 2020).

389 In contrast to a holistic simulation, such a segmented simulation approach undoubtedly causes poor articulation
390 and increased uncertainty in different processes. With the recent scientific developments, a newly developed three-
391 phase flow model, r.avaflow (Mergili et al., 2017), started to be used to simulate GLOF propagations (Mergili et al.,
392 2018, 2020; [Sattar et al., 2023](#)) and can realize the whole hazard cascade modeling with a high performance (Zheng
393 et al., 2021). Our study can provide much-needed glacial lake bathymetry data for such modeling to calculate the
394 displacement wave in the lake surface and the water release process during dam erosion.

395 **4.5 Potential developments of numerical or physical models**

396 The standardized glacial lake basin can facilitate other future model development related to glacial lakes and
397 improve knowledge of how the proglacial lakes and lake-terminating glaciers interact. Carrivick et al. (2020)
398 discussed six major challenges in constructing a numerical model of interactions between proglacial lakes and
399 glaciers, which include the imperative for glacial lake bathymetry. The standardized shape implicates the design of
400 the model's basic architecture.

401 Compared with the somewhat realistic glacier bed topography within the overdeepenings revealed by Ice
402 Thickness Models, a standardized lake basin provides an alternative scheme. For a specific proglacial lake, its water
403 level, water temperature, in/outflow, internal circulation, and interface with the glacier vary with glacier-lake

404 dynamics and time, which are very complex processes (Sugiyama et al., 2016; Sutherland et al., 2020). Deep and
405 large proglacial lakes are prone to water stratification due to warmer upper layers and colder lower layers of water
406 because these freshwater terminating lakes currently have no evidence of active internal circulation (Haresign and
407 Warren, 2005; Boyce et al., 2007). This stratification induces the subaqueous ice differential melting and ice terrace
408 formation (Fig. 9b), impacting the glacier terminal calving regimes (Sugiyama et al., 2019; Mallalieu et al., 2020).
409 On the other hand, the dynamic characteristics of glacier snout, such as bed friction, longitudinal stress, and ice flow
410 velocity, vary distinctively due to the presence of terminating lakes (Sugiyama et al., 2011; Liu et al., 2020). The
411 knowledge and understanding of glacial lakes formation and evolution changes continually. The ultimate goal is to
412 present these processes via computer numerical simulations. Yet, the idealized lake basin can facilitate calculating
413 the mass and energy transport at the interface.

414

415 **5 Conclusion**

416 This study was conducted in response to a circumstance that field investigation was the only approach to obtain
417 glacial lake bathymetry. The relationships of volume–area and maximum water depth–area of glacial lakes were
418 reanalyzed via an inventory of the global glacial lake bathymetry data we compiled. The obtained curves were
419 matched with a power-law relationship. Thus, the types of hemispheres or cones were determined as the conceptual
420 models (idealized geometric shapes) of glacial lakes. The standard lake surface was assumed to be an ellipse.

421 Nine standard conceptual models were identified. The SCMs for the supraglacial, periglacial, and extraglacial
422 lakes are the hemisphere structured by the elliptical side; the hemisphere structured by the upward-opening parabolic
423 side; the cone structured by the straight side; and the cone structured by the rightward-opening parabolic side. The
424 SCMs for the proglacial lakes were determined to be half of the aforementioned four SCMs. Two SCMs were
425 considered for the ice-dammed lakes: the semi–cone structured by the straight side and the triangular cone. To depict
426 the volume between the two SCMs, a general conceptual model was defined to represent the transition from one
427 SCM to another.

428 Several hypotheses are important in our algorithm to nest the actual glacial lake shapes from idealized
429 conceptual models and interpolate glacial lake bathymetric distribution. First, the supraglacial, periglacial, and
430 extraglacial lakes' deepest sites were assumed to be in the lake center, whereas the proglacial lakes and ice-dammed
431 lakes' deepest sites were near the glacier-lake interface. Second, the effects of exogenous materials and boundary

432 conditions were used to explain the different rates of inward deepening of glacial lakes. Six glacial lakes with
433 measured bathymetry data were selected in the Third Pole region for comparison with the simulated bathymetric
434 distributions. The results demonstrated good accuracy and applicability of our conceptual models in estimating lake
435 bathymetry. Relatively high consistency was shown in the point-to-point comparisons of the measured and simulated
436 water depths. This study constructed the glacial lake bathymetric distribution model which is very rewarding for
437 comprehending the evolution of glacial lakes. Moreover, the quality of GLOF modeling and risk assessment is also
438 enhanced by our outlined general conceptual model. These standardized lake basins implicate the design of the
439 model's basic architecture, which can potentially promote the development of future numerical or physical models
440 of glacial lakes.

441

442 *Code availability.* The codes for calculating the functional equations of a general conceptual model in the coordinate
443 axes are available on request.

444 *Data availability.* The observed bathymetric data of Jialongco and Longbasaba Lake were provided by Dr. Xiaojun
445 Yao and Donghui Shangguan, respectively. The observed bathymetric data of Poiqu NO.1, Dasuopuco, and
446 Maqiongco can be freely downloaded at <https://doi.org/10.6084/m9.figshare.21569175> (Zhang et al., 2023).

447 *Supplement.* The supplement related to this article is available online at: <https://tc.copernicus.org/preprints/tc-2023-12/tc-2023-12-supplement.zip>.

449 *Author contributions.* TZ and WW designed the study, compiled the data and drafted the manuscript. BA revised and
450 edited the manuscript.

451 *Competing interests.* The authors declare that they have no conflict of interest.

452 *Acknowledgements.* We thank the two anonymous reviewers, Dr. Adam Emmer and the editor, Xichen Li, for the
453 constructive comments that improved the paper.

454 *Financial support.* This study was supported by the Second Tibetan Plateau Scientific Expedition and Research
455 (STEP) Program (2019QZKK0208); ~~the Strategic Priority Research Program of the Chinese Academy of Sciences~~
456 ~~(XDA20100300);~~—and the International Partnership Program of Chinese Academy of Sciences
457 (131C11KYSB20200029).

459 **References**

- 460 Aggarwal, S., Rai, S. C., Thakur, P. K., and Emmer, A.: Inventory and recently increasing GLOF susceptibility of glacial lakes in Sikkim,
461 Eastern Himalaya, *Geomorphology*, 295, 39–54, <http://dx.doi.org/10.1016/j.geomorph.2017.06.014>, 2017.
- 462 Alho, P., and Aaltonen, J.: Comparing a 1D hydraulic model with a 2D hydraulic model for the simulation of extreme glacial outburst
463 floods, *Hydrol. Process*, 22, 1537–1547. <http://dx.doi.org/10.1002/hyp.6692>, 2018.
- 464 Allen, S. K., Rastner, P., Arora, M., Huggel, C., and Stoffel, M. (2016). Lake outburst and debris flow disaster at Kedarnath, June 2013:
465 hydrometeorological triggering and topographic predisposition, *Landslides*, 13, 1479–1491, [http://dx.doi.org/10.1007/s10346-015-](http://dx.doi.org/10.1007/s10346-015-0584-3)
466 0584-3, 2015.
- 467 Anaconda, P. I., Mackintosh, A., Norton, K. P.: Hazardous processes and events from glacier and permafrost areas: lessons from the
468 Chilean and Argentinean Andes, *Earth Surf. Process Landf.*, 40, 2–21, <http://dx.doi.org/10.1002/esp.3524>, 2015a.
- 469 Anaconda, P. I., Mackintosh, A., Norton, K.: Reconstruction of a glacial lake outburst flood (GLOF) in the Engano Valley, Chilean
470 Patagonia: Lessons for GLOF risk management, *Sci. Total Environ.*, 527–528, 1–11,
471 <http://dx.doi.org/10.1016/j.scitotenv.2015.04.096>, 2015b.
- 472 Bolch, T., Buchroithner, M. F., Peters, J., Pradhan, B., Buchroithner, M., and Blagoveshchensky, V.: Identification of glacier motion and
473 potentially dangerous glacial lakes in the mt. Everest region/Nepal using spaceborne imagery, *Nat. Hazard Earth Syst.*, 8, 1329–
474 1340, <http://dx.doi.org/10.1007/s11069-011-9860-2>, 2011.
- 475 Boyce, E. S., Motyka, R. J., and Truffer, M.: Flotation and retreat of a lake-calving terminus, Mendenhall Glacier, southeast Alaska,
476 USA, *J. of Glaciol.*, 53, 211–224, <http://dx.doi.org/10.3189/172756507782202928>, 2007.
- 477 Carrivick, J. L., and Tweed, F. S.: Proglacial lakes: character, behaviour and geological importance, *Quat. Sci. Rev.*, 78, 34–52,
478 <http://dx.doi.org/10.1016/j.quascirev.2013.07.028>, 2013.
- 479 Carrivick, J. L., and Tweed, F. S.: A global assessment of the societal impacts of glacier outburst floods, *Glob. Planet. Change*, 144, 1–
480 16, <http://dx.doi.org/10.1016/j.gloplacha.2016.07.001>, 2016.
- 481 Carrivick, J. L., Tweed, F. S., Sutherland, J. L., and Mallalieu, J.: Toward numerical modeling of interactions between ice-marginal
482 proglacial lakes and glaciers, *Front. Earth Sci.*, 500, <https://doi.org/10.3389/feart.2020.577068>, 2020.
- 483 Cook, S. J., Quincey, D. J.: Estimating the volume of Alpine glacial lakes, *Earth Surf. Dyn.*, 3, 559–575, [http://www.earth-surf-](http://www.earth-surf-dynam.net/3/559/2015/doi:10.5194/esurf-3-559-2015)
484 [dynam.net/3/559/2015/doi:10.5194/esurf-3-559-2015](http://www.earth-surf-dynam.net/3/559/2015/doi:10.5194/esurf-3-559-2015), 2015.
- 485 Coulombe, S., Fortier, D., Bouchard, F., Paquette, M., Charbonneau, S., Lacelle, D., Laurion, I. and Pienitz, R. Contrasted
486 geomorphological and limnological properties of thermokarst lakes formed in buried glacier ice and ice-wedge polygon terrain,
487 *Cryosphere*, 16, 2837–2857. <https://doi.org/10.5194/tc-16-2837-2022>, 2022.
- 488 Drenkhan, F., Huggel, C., Guardamino, L., and Haerberli, W.: Managing risks and future options from new lakes in the deglaciating
489 Andes of Peru: The example of the Vilcanota-Urubamba basin, *Sci. Total Environ.*, 665, 465–483,
490 <https://doi.org/10.1016/j.scitotenv.2019.02.070>, 2019.
- 491 [Duan, H., Yao, X., Zhang, Y., Jin, H., Wang, Q., Du, Z., Hu, J., Wang, B., and Wang, Q.: Lake volume and potential hazards of moraine-](https://doi.org/10.5194/tc-17-591-2023)
492 [dammed glacial lakes—a case study of Bienong Co, southeastern Tibetan Plateau. *Cryosphere*, 17, 591–616,](https://doi.org/10.5194/tc-17-591-2023)
493 <https://doi.org/10.5194/tc-17-591-2023>, 2023.
- 494 Echelmeyer, K., Wang Z. X.: Direct observation of basal sliding and deformation of basal drift at sub-freezing temperatures, *J. Glaciol.*,
495 33, 83–98. <http://dx.doi.org/10.3189/s0022143000005396>, 1987.
- 496 Emmer, A., and Vilímek, V.: New method for assessing the susceptibility of glacial lakes to outburst floods in the Cordillera Blanca,
497 Peru, *Hydrol. Earth Syst. Sci.*, 18, 3461–3479, <http://www.hydrol-earth-syst-sci.net/18/3461/2014/doi:10.5194/hess-18-3461-2014>,
498 2014.
- 499 Emmer, A., Klimeš, J., Mergili, M., Vilímek, V. and Cochachin, A.: 882 lakes of the Cordillera Blanca: An inventory, classification,

500 evolution and assessment of susceptibility to outburst floods, *Catena*, 147, 269–279, <http://dx.doi.org/10.1016/j.catena.2016.07.032>,
501 2016.

502 Emmer, A., Allen, S.K., Carey, M., Frey, H., Huggel, C., Korup, O., Mergili, M., Sattar, A., Veh, G., Chen, T.Y., Cook, S.J., Correas-
503 Gonzalez, M., Das, S., Diaz Moreno, A., Drenkhan, F., Fischer, M., Immerzeel, W.W., Izagirre, E., Joshi, R.C., Kougkoulos, I.,
504 Kuyakanon Knapp, R., Li, D., Majeed, U., Matti, S., Moulton, H., Nick, F., Piroton, V., Rashid, I., Reza, M., Ribeiro de Figueiredo,
505 A., Riveros, C., Shrestha, F., Shrestha, M., Steiner, J., Walker-Crawford, N., Wood, J.L. and Yde, J.C. Progress and challenges in
506 glacial lake outburst flood research (2017–2021): a research community perspective, *Nat. Hazard Earth Sys. Sci.*, 22, 3041–3061.
507 <https://doi.org/10.5194/nhess-22-3041-2022>, 2022a.

508 Emmer, A., Wood, J.L., Cook, S.J., Harrison, S., Wilson, R., Diaz-Moreno, A., Reynolds, J.M., Torres, J.C., Yarleque, C., Mergili, M.,
509 Jara, H.W., Bennett, G., Caballero, A., Glasser, N.F., Melgarejo, E., Riveros, C., Shannon, S., Turpo, E., Tinoco, T., Torres, L.,
510 Garay, D., Villafane, H., Garrido, H., Martinez, C., Apaza, N., Araujo, J. and Poma, C. 160 glacial lake outburst floods (GLOFs)
511 across the Tropical Andes since the Little Ice Age, *Global Plane. Change*, 208. <https://doi.org/10.1016/j.gloplacha.2021.103722>,
512 2022b.

513 Erokhin, S. A., Zaginaev, V. V., Meleshko, A. A., Ruiz-Villanueva, V., Petrakov, D. A., Chernomorets, S. S., Viskhadzheva, K. S.,
514 Tutubalina, O. V., and Stoffel, M.: Debris flows triggered from non-stationary glacier lake outbursts: the case of the Teztor Lake
515 complex (Northern Tian Shan, Kyrgyzstan), *Landslides*, 15, 83–98, <http://dx.doi.org/10.1007/s10346-017-0862-3>, 2018.

516 Evans, S. G.: The maximum discharge of outburst floods caused by the breaching of man-made and natural dams, *Can. Geotech. J.*,
517 23(3), 385–387, <http://dx.doi.org/10.1139/t87-062>, 1986.

518 Evers F. M., Heller, V., Fuchs, H., Hager, W. H., and Boes, R. M.: *Landslide-generated Impulse Waves in Reservoirs: Basics and*
519 *Computation*, VAW-Mitteilungen, 254, 2019.

520 Falatkova, K., Šobr, M., Neureiter, A., Schöner, W., Janský, B., Häusler, H., Engel, Z., and Beneš, V.: Development of proglacial lakes
521 and evaluation of related outburst susceptibility at the Adygin ice-debris complex, northern Tien Shan, *Earth Surf. Dyn.*, 7, 301–
522 320, <https://doi.org/10.5194/esurf-7-301-2019>, 2019.

523 Field, H. R., Armstrong, W. H. and Huss, M.: Gulf of Alaska ice-marginal lake area change over the Landsat record and potential physical
524 controls, *Cryosphere*, 15, 3255–3278. <https://doi.org/10.5194/tc-15-3255-2021>, 2021.

525 Frey, H., Huggel, C., Chisolm, R. E., Baer, P., McArdeell, B., Cochachin, A., and Portocarrero, C.: Multi-source glacial lake outburst
526 flood hazard assessment and mapping for Huaraz, Cordillera Blanca, Peru, *Front. Earth Sci.*, 6, 210.
527 <https://doi.org/10.3389/feart.2018.00210>, 2018.

528 Fujita, K., Sakai, A., Takenaka, S., Nuimura, T., Surazakov, A. B., Sawagaki, T., and Yamanokuchi, T.: Potential flood volume of
529 Himalayan glacial lakes, *Nat. Hazard Earth Syst. Sci.*, 13, 1827–1839, [http://www.nat-hazards-earth-syst-
530 sci.net/13/1827/2013/doi:10.5194/nhess-13-1827-2013](http://www.nat-hazards-earth-syst-sci.net/13/1827/2013/doi:10.5194/nhess-13-1827-2013), 2013.

531 [Gu, C., Li, S., Liu, M., Hu, K., and Wang, P.: Monitoring Glacier Lake Outburst Flood \(GLOF\) of Lake Merzbacher Using Dense Chinese
532 High-Resolution Satellite Images. *Remote Sens.*, 15, <https://doi.org/10.3390/rs15071941>, 2023.](https://doi.org/10.3390/rs15071941)

533 Haresign, E., and Warren, C. R.: Melt rates at calving termini: a study at Glaciar León, Chilean Patagonia, *Geological Society, London,*
534 *Special Publications*, 242, 99–109, <http://dx.doi.org/10.1144/GSL.SP.2005.242.01.09>, 2005.

535 Heller, V., Hager, W. H., Minor, H. E.: *Landslide Generated Impulse Waves in Reservoirs*, Zurich: Mitteilungen Versuchsanstalt für
536 *Wasserbau, Hydrologie und Glaziologie (VAW)*, ETH Zürich, 2019.

537 Huggel, C., Kääh, A., Haerberli, W., Haerberli, W., Teyssie, P., and Paul, F.: Remote sensing based assessment of hazards from glacier
538 lake outbursts: a case study in the Swiss Alps, *Can. Geotech. J.*, 39, 316–330, <http://dx.doi.org/10.1139/t01-099>, 2002.

539 Hugonnet, R., McNabb, R., Berthier, E., Menounos, B., Nuth, C., Girod, L., Farinotti, D., Huss, M., Dussailant, I., Brun, F., and Kääh,
540 A.: Accelerated global glacier mass loss in the early twenty-first century, *Nature*, 592, 726–731, [https://doi.org/10.1038/s41586-
541 021-03436-z](https://doi.org/10.1038/s41586-021-03436-z), 2021.

542 Kapitsa, V., Shahgedanova, M., Machguth, H., Severskiy, I., and Medeu, A.: Assessment of evolution and risks of glacier lake outbursts
543 in the Djungarskiy Alatau, Central Asia, using Landsat imagery and glacier bed topography modelling, *Nat. Hazard Earth Syst. Sci.*,

544 17, 1837–1856, <https://doi.org/10.5194/nhess-17-1837-2017>, 2017.

545 Khanal, N. R., Hu, J. M., and Mool, P.: Glacial lake outburst flood risk in the Poiqu/Bhote Koshi/Sun Koshi river basin in the Central
546 Himalayas, *Mt. Res. Dev.*, 35, 351–364, <http://dx.doi.org/10.1659/MRD-JOURNAL-D-15-00009>, 2015.

547 Kougkoulos, I., Cook, S. J., Edwards, L. A., Clarke, L. J., Symeonakis, E., Dortch, J. M., and Nesbitt, K.: Modelling glacial lake outburst
548 flood impacts in the Bolivian Andes, *Nat. Hazard*, 94, 1415–1438, <https://doi.org/10.1007/s11069-018-3486-6>, 2018.

549 Li, D., Shangguan, D. H., Wang, X., Ding, Y. J., Su, P. C., Liu, R. L., and Wang, M. X.: Expansion and hazard risk assessment of glacial
550 lake Jialong Co in the central Himalayas by using an unmanned surface vessel and remote sensing, *Sci. Total Environ.*, 784,
551 <https://doi.org/10.1016/j.scitotenv.2021.147249>, 2021.

552 Linsbauer, A., Frey, H., Haeberli, W., Machguth, H., Azam, M. F., and Allen, S.: Modelling glacier-bed overdeepenings and possible
553 future lakes for the glaciers in the Himalaya—Karakoram region, *Ann. Glaciol.*, 57, 119–130,
554 <http://dx.doi.org/10.3189/2016AoG71A627>, 2016.

555 Liu, Q., Mayer, C., Wang, X., Nie, Y., Wu, K. P., Wei, J. F., and Liu, S. Y.: Interannual flow dynamics driven by frontal retreat of a lake-
556 terminating glacier in the Chinese Central Himalaya, *Earth Planet. Sci. Lett.*, 546, 116450,
557 <https://doi.org/10.1016/j.epsl.2020.116450>, 2020.

558 Lliboutry, L., Arnao, B. M., Pautre, A., and Schneider, B.: Glaciological problems set by the control of dangerous lakes in Cordillera
559 Blanca, Peru. I. Historical failures of morainic dams, their causes and prevention, *J. Glaciol.*, 18, 239–254,
560 <http://dx.doi.org/10.1017/S002214300002133X>, 1977.

561 Loriaux, T., Casassa, G.: Evolution of glacial lakes from the Northern Patagonia Icefield and terrestrial water storage in a sea-level rise
562 context, *Glob. Planet. Change*, 102, 33–40, <http://dx.doi.org/10.1016/j.gloplacha.2012.12.012>, 2013.

563 Lützwow, N., Veh, G. and Korup, O. A global database of historic glacier lake outburst floods, *Earth Sys. Sci. Data*, (in discussion).
564 <http://dx.doi.org/10.5194/essd-2022-449>, 2023.

565 Ma, J. S., Song, C. Q., Wang, Y. J.: Spatially and Temporally Resolved Monitoring of Glacial Lake Changes in Alps During the Recent
566 Two Decades, *Front. Earth Sci.*, 9, <https://doi.org/10.3389/feart.2021.723386>, 2021.

567 Mallalieu, J., Carrivick, J. L., Quincey, D. J., and Smith, M. W.: Calving seasonality associated with melt-undercutting and lake ice
568 cover, *Geophys. Res. Lett.*, 47, e2019GL086561, <https://doi.org/10.1029/2019GL086561>, 2020.

569 Maurer, J. M., Schaefer, J. M., Russell, J. B., Rupper, S., Wangdi, N., Putnam, A. E., and Young, N.: Seismic observations, numerical
570 modeling, and geomorphic analysis of a glacier lake outburst flood in the Himalayas, *Sci. Adv.*, 6, eaba3645,
571 <http://dx.doi.org/10.1126/sciadv.aba3645>, 2020.

572 Mergili, M., Fischer, J. T., Krenn, J., Pudasaini, S. P.: r. avaflow v1, an advanced open-source computational framework for the
573 propagation and interaction of two-phase mass flows, *Geosci. Model Develop.*, 10, 553–569, <http://dx.doi.org/10.5194/gmd-10-553-2017>, 2017.

574

575 Mergili, M., Emmer, A., Juricova, A., Cochachin, A., Fischer, G. T., Huggel, C., and Pudasaini, S. P.: How well can we simulate complex
576 hydro-geomorphic process chains? The 2012 multi-lake outburst flood in the Santa Cruz Valley (Cordillera Blanca, Peru), *Earth
577 Surf. Process. Landf.*, 431373–1389, <http://dx.doi.org/10.1002/esp.4318>, 2018.

578 Mergili M, Pudasaini SP, Emmer A, Fischer, G. T., Cochachin, A., Frey, H.: Reconstruction of the 1941 GLOF process chain at Lake
579 Palcacocha (Cordillera Blanca, Peru), *Hydrol. Earth Syst. Sci.*, 24, 93–114, <https://doi.org/10.5194/hess-24-93-2020>, 2020.

580 [Mertes, J. R., Thompson, S. S., Booth, A. D., Gulley, J. D., and Benn, D. I.: A conceptual model of supra-glacial lake formation on
581 debris-covered glaciers based on GPR facies analysis. *Earth Surf. Process. Landf.*, 42, 903–914, <http://dx.doi.org/10.1002/esp.4068>,
582 2017.](https://doi.org/10.1002/esp.4068)

583 Miles, E. S., Watson, C. S., Brun, F., Berthier, E., Esteves, M., Quincey, D. J., Miles, K. E., Hubbard, B., and Wagnon, P.: Glacial and
584 geomorphic effects of a supraglacial lake drainage and outburst event, Everest region, Nepal Himalaya, *The Cryosphere*, 12, 3891–
585 3905, <https://doi.org/10.5194/tc-12-3891-2018>, 2018.

586 [Minowa, M., Schaefer, M., and Skvarca, P.: Effects of topography on dynamics and mass loss of lake-terminating glaciers in southern
587 Patagonia. *J. Glaciol.*, 1–18. <https://doi.org/10.1017/jog.2023.42>, 2023.](https://doi.org/10.1017/jog.2023.42)

588 Muñoz, R., Huggel, C., Frey, H., Cochachin, A., and Haeblerli, W.: Glacial lake depth and volume estimation based on a large bathymetric
589 dataset from the Cordillera Blanca, Peru, *Earth Surf. Process. Landf.*, <http://dx.doi.org/10.1002/esp.4826>, 2020.

590 Nie, Y., Liu, Q., Wang, J. D., Zhang, Y. L., Sheng, Y. W., and Liu, S. Y.: An inventory of historical glacial lake outburst floods in the
591 Himalayas based on remote sensing observations and geomorphological analysis, *Geomorphology*, 308, 91–106,
592 <https://doi.org/10.1016/j.geomorph.2018.02.002>, 2018.

593 Nie, Y., Liu, W., Liu, Q., Hu, X., and Westoby, M. J.: Reconstructing the Chongbaxia Tsho glacial lake outburst flood in the Eastern
594 Himalaya: Evolution, process and impacts, *Geomorphology*, 370, 107393, <https://doi.org/10.1016/j.geomorph.2020.107393>, 2020.

595 O'Connor, J. E., Hardison III, J. H., Costa, J. E.: *Debris Flows from Failures of Neoglacial-Age Moraine Dams in the Three Sisters and*
596 *Mount Jefferson Wilderness Areas, Oregon*, 105 pp, 2001.

597 Osti, R., and Egashira, S.: Hydrodynamic characteristics of the Tam Pokhari glacial lake outburst flood in the Mt. Everest region, Nepal,
598 *Hydrol. Process.*, 23, 2943–2955, <http://dx.doi.org/10.1002/hyp.7405>, 2009.

599 Patel, L. K., Sharma, P., Laluraj, C. M., Thamban, M., Singh, A., and Ravindra, R.: A geospatial analysis of Samudra Tapu and Gepang
600 Gath glacial lakes in the Chandra Basin, Western Himalaya, *Nat. Hazard*, 86, 1275–1290,
601 <https://link.springer.com/article/10.1007/s11069-017-2743-4>, 2017.

602 Petrov, M. A., Sabitov, T. Y., Tomashevskaya, I. G., Glazirin, G. E., Chernomorets, S. S., Savernyuk, E. A., Tutubalina, O. V., Petrakov,
603 D. A., Sokolov, L. S., Dokukin, M. D., Mountrakis, G., Ruiz-Villanueva, V., and Stoffel, M.: Glacial lake inventory and lake outburst
604 potential in Uzbekistan, *Sci. Total Environ.*, 592, 228–242, <http://dx.doi.org/10.1016/j.scitotenv.2017.03.068>, 2017.

605 Qi, M. M., Liu, S. Y., Wu, K. P., Zhu, Y., Xie, F. M., Jin, H., Gao, Y. P. and Yao, X. J. Improving the accuracy of glacial lake volume
606 estimation: A case study in the Poiqu basin, central Himalayas, *J. Hydrol.*, 610, <https://doi.org/10.1016/j.jhydrol.2022.127973>, 2022.

607 Rick, B., McGrath, D., Armstrong, W. and McCoy, S.W. Dam type and lake location characterize ice-marginal lake area change in Alaska
608 and NW Canada between 1984 and 2019, *Cryosphere*, 16, 297–314. <https://doi.org/10.5194/tc-16-297-2022>, 2022.

609 Richardson, S. D., Reynolds, J. M.: An overview of glacial hazards in the Himalayas, *Quat. Int.*, 65–6, 31–47,
610 [http://dx.doi.org/10.1016/S1040-6182\(99\)00035-X](http://dx.doi.org/10.1016/S1040-6182(99)00035-X), 2000.

611 Sakai, A.: Glacial lakes in the Himalayas: a review on formation and expansion processes, *Glob. Environ. Res.*, 16, 23–30, 2012.

612 Sattar, A., Haritashya, U. K., Kargel, J. S., Leonard, G. J., Shugar, D. H., and Chase, D. V.: Modeling lake outburst and downstream
613 hazard assessment of the Lower Barun Glacial Lake, Nepal Himalaya, *J. Hydrol.*, 598, 126208.
614 <https://doi.org/10.1016/j.jhydrol.2021.126208>, 2021.

615 [Sattar, A., Allen, S., Mergili, M., Haeblerli, W., Frey, H., Kulkarni, A. V., Haritashya, U. K., Huggel, C., Goswami, A., and Ramsankaran,](#)
616 [R.: Modeling Potential Glacial Lake Outburst Flood Process Chains and Effects From Artificial Lake-Level Lowering at Gepang](#)
617 [Gath Lake, Indian Himalaya. *J. Geophys. Res. Earth Surf.*, 128, <https://doi.org/10.1029/2022JF006826>, 2023.](#)

618 Schneider, D., Huggel, C., Cochachin, A., Guillén, S., and García, J.: Mapping hazards from glacier lake outburst floods based on
619 modelling of process cascades at Lake 513, Carhuaz, Peru, *Adv. Geosci.*, 35, 145–155, [http://dx.doi.org/10.5194/adgeo-35-145-](http://dx.doi.org/10.5194/adgeo-35-145-2014)
620 2014, 2014.

621 Sharma, R. K., Pradhan, P., Sharma, N. P., and Shrestha, D. G.: Remote sensing and in situ-based assessment of rapidly growing South
622 Lhonak glacial lake in eastern Himalaya, India, *Nat. Hazard*, 93, 393–409, <https://doi.org/10.1007/s11069-018-3305-0>, 2018.

623 Shugar, D. H., Burr, A., Haritashya, U. K., Kargel, J. S., Watson, C. S., Kennedy, M. C., Bevington, A. R., Betts, R. A., Harrison, S., and
624 Strattman, K.: Rapid worldwide growth of glacial lakes since 1990, *Nat. Clim. Change*, 10, 939–945,
625 <https://doi.org/10.1038/s41558-020-0855-4>, 2020.

626 [Singh, H., Varade, D., de Vries, M.V.W., Adhikari, K., Rawat, M., Awasthi, S., Rawat, D.: Assessment of potential present and future](#)
627 [glacial lake outburst flood hazard in the Hunza valley: A case study of Shisper and Mochowar glacier, *Sci. Total Environ.*, 868,](#)
628 [161717, <https://doi.org/10.1016/j.scitotenv.2023.161717>, 2023.](#)

629 Somos-Valenzuela, M. A., McKinney, D. C., Byers, A. C., Rounce, D. R., Portocarrero, C., and Lamsal, D.: Assessing downstream flood
630 impacts due to a potential GLOF from Imja Tsho in Nepal, *Hydrol. Earth Syst. Sci.*, 19, 1401–1412, [http://dx.doi.org/10.5194/hess-](http://dx.doi.org/10.5194/hess-19-1401-2015)
631 19-1401-2015, 2015.

632 Sugiyama, S., Skvarca, P., Naito, N., Enomoto, H., Tsutaki, S., Tone, K., Marinsek, S., and Aniya, M.: Ice speed of a calving glacier
633 modulated by small fluctuations in basal water pressure, *Nat. Geosci.*, 4, 597–600, <http://dx.doi.org/10.1038/ngeo1218>, 2011.

634 Sugiyama, S., Minowa, M., Sakakibara, D., Skvarca, P., Sawagaki, T., Ohashi, Y., Naito, N., and Chikita, K.: Thermal structure of
635 proglacial lakes in Patagonia, *J. Geophys. Res.: Earth Surf.*, 121, 2270–2286, <http://dx.doi.org/10.1002/2016JF004084>, 2016.

636 Sugiyama, S., Minowa, M., and Schaefer, M.: Underwater ice terrace observed at the front of Glacier Grey, a freshwater calving glacier
637 in Patagonia, *Geophys. Res. Lett.*, 46, 2602–2609, <http://dx.doi.org/10.1029/2018GL081441>, 2019.

638 Sugiyama, S., Minowa, M., Fukamachi, Y., Hata, S., Yamamoto, Y., Sauter, T., Schneider, C., and Schaefer, M.: Subglacial discharge
639 controls seasonal variations in the thermal structure of a glacial lake in Patagonia, *Nat. Commun.*, 12, 1–9,
640 <https://doi.org/10.1038/s41467-021-26578-0>, 2021.

641 Sutherland, J. L., Carrivick, J. L., Gandy, N., Shulmeister, J., Quincey, D. J., and Cornford, S. L.: Proglacial lakes control glacier
642 geometry and behavior during recession, *Geophys. Res. Lett.*, 47, e2020GL088865, <https://doi.org/10.1029/2020GL088865>, 2020.

643 Veh, G., Korup, O., and Walz, A.: Hazard from Himalayan glacier lake outburst floods, *PNAS*, 117, 907–912,
644 <https://www.pnas.org/cgi/doi/10.1073/pnas.1914898117>, 2020.

645 Wang, X., Liu, S. Y., Ding, Y. J., Guo, W. Q., Jiang, Z. L., Lin, J., and Han, Y.: An approach for estimating the breach probabilities of
646 moraine-dammed lakes in the Chinese Himalayas using remote-sensing data, *Nat. Hazard Earth Syst. Sci.*, 12, 3109–3122,
647 <http://dx.doi.org/10.5194/nhess-12-3109-2012>, 2012.

648 Wang, X., Guo, X. Y., Yang C. D., Liu, Q. H., Wei, J. F., Zhang, Y., Liu, S. Y., Zhang, Y. L., Jiang, Z. L., and Tang, Z. G.: Glacial lake
649 inventory of high-mountain Asia in 1990 and 2018 derived from Landsat images, *Earth Syst. Sci. Data*, 12, 2169–2182,
650 <https://doi.org/10.5194/essd-12-2169-2020>, 2020.

651 Wang, W. C., Gao, Y., Anaconda, P. I., Lei, Y. B., Xiang, Y., Zhang, G. Q., Li, S. H., and Lu, A. X.: Integrated hazard assessment of
652 Cirenmaco glacial lake in Zhangzangbo valley, Central Himalayas, *Geomorphology*, 306, 292–305,
653 <http://dx.doi.org/10.1016/j.geomorph.2015.08.013>, 2018.

654 Watson, C. S., Quincey, D. J., Carrivick, J. L., Smith, M. W., Rowan, A. V., and Richardson, R.: Heterogeneous water storage and thermal
655 regime of supraglacial ponds on debris-covered glaciers, *Earth Surf. Process. Landf.*, 43, 229–241,
656 <http://dx.doi.org/10.1002/esp.4236>, 2018.

657 Watson, C. S., Kargel, J. S., Shugar, D. H., Haritashya, U. K., Schiassi, E., and Furfaro, R. Mass Loss From Calving in Himalayan
658 Proglacial Lakes *Front. Earth Sci.* 7, 342, <http://dx.doi.org/10.3389/feart.2019.00342>, 2020.

659 [Wei, J., Liu, S., Wang, X., Zhang, Y., Jiang, Z., Wu, K., Zhang, Z., and Zhang, T.: Longbasaba Glacier recession and contribution to its
660 proglacial lake volume between 1988 and 2018. *J. Glaciol.*, 1–12, <https://doi.org/10.1017/jog.2020.119>, 2021.](https://doi.org/10.1017/jog.2020.119)

661 Westoby, M. J., Glasser, N. F., Brasington, J., Hambrey, M. J., Quincey, D. J., and Reynolds, J. M.: Modelling outburst floods from
662 moraine-dammed glacial lakes, *Earth-Sci. Rev.*, 134, 137–159, <http://dx.doi.org/10.1016/j.earscirev.2014.03.009>, 2014.

663 Wood, J. L., Harrison, S., Wilson, R., Emmer, A., Yarleque, C., Glasser, N. F., Torres, J. C., Caballero, A., Araujo, J., Bennett, G. L.,
664 Diaz-Moreno, A., Garay, D., Jara, H., Poma, C., Reynolds, J. M., Riveros, C. A., Romero, E., Shannon, S., Tinoco, T., Turpo, E.,
665 and Villafane, H.: Contemporary glacial lakes in the Peruvian Andes, *Glob. Planet. Change*, 204, 103574,
666 <https://doi.org/10.1016/j.gloplacha.2021.103574>, 2021.

667 Yao, T. D., Thompson, L., Yang, W., Yu, W. S., Gao, Y., Guo, X. J., Yang, X. X., Duan, K. Q., Zhao, H. B., Xu, B. Q., Pu, J. C., Lu, A.
668 X., Xiang, Y., Kalltel, D. B., and Joswiak, D.: Different glacier status with atmospheric circulations in Tibetan Plateau and
669 surroundings, *Nat. Clim. Change*, 2, 663–667, <http://www.nature.com/doi/10.1038/nclimate1580>, 2012.

670 Yao, T. D., Xue, Y. K., Chen, D. L., Chen, F. H., Thompson, L., Cui, P., Koike, T., K.-M. Lau, W., Lettenmaier, D., Mosbrugger, V.,
671 Zhang, R. H., Xu, B. Q., Dozier, J., Gillespie, T., Gu, Y., Kang, S. C., Piao, S. L., Sugimoto, S., Ueno, K., Wang, L., Wang, W. C.,
672 Zhang, F., Sheng, Y. W., Guo, W. D., Ailikun, Yang, X. X., Ma, Y. M., Shen, S. S. P., Su, Z. B., Chen, F., Liang, S. L., Liu, Y. M.,
673 Singh, V. P., Yang, K., Yang, D. Q., Zhao, X. Q., Qian, Y., Zhang, Y., and Li, Q.: Recent third pole’s rapid warming accompanies
674 cryospheric melt and water cycle intensification and interactions between monsoon and environment: Multidisciplinary approach
675 with observations, modeling, and analysis, *B. Am. Meteorol. Soc.*, 100, 423–444, <https://doi.org/10.1175/BAMS-D-17-0057.1>,

676 2019.

677 Yao, X. J., Liu, S. Y., Sun, M. P., Wei, J. F., and Guo, W. Q.: Volume calculation and analysis of the changes in moraine-dammed lakes
678 in the north Himalaya: a case study of Longbasaba lake, *J. Glaciol.*, 58, 753–760, <http://dx.doi.org/10.3189/2012JoG11J048>, 2012.

679 Yao, X. J., Liu, S. Y., Han, L., Sun, M. P., and Zhao, L. L.: Definition and classification system of glacial lake for inventory and hazards
680 study, *J. Geogr. Sci.*, 28, 193–205, <https://doi.org/10.1007/s11442-018-1467-z>, 2018.

681 Zemp, M., Huss, M., Thibert, E., McNabb, R., Huber, J., Barandun, M., Machguth, H., Nussbaumer, S. U., Gärtner-roer, I., Thomson,
682 L., Paul, F., Maussion, F., Kutuzov, S., and Cogley, J. G.: Global glacier mass changes and their contributions to sea-level rise from
683 1961 to 2016, *Nature*, 568, 382–386, <https://doi.org/10.1038/s41586-019-1071-0>, 2019.

684 Zhang, G. Q., Yao, T. D., Xie, H. J., Wang, W. C., and Yang, Wei.: An inventory of glacial lakes in the Third Pole region and their changes
685 in response to global warming, *Glob. Planet. Change*, 131, 148–157, <http://dx.doi.org/10.1016/j.gloplacha.2015.05.013>, 2015.

686 Zhang, G. Q., Bolch, T., Yao, T. D., Rounce, D.R., Chen, W. F., Veh, G., King, O., Allen, S.K., Wang, M. and Wang, W. C. Underestimated
687 mass loss from lake-terminating glaciers in the greater Himalaya, *Nat. Geosci.*, 16, 1–6. [https://doi.org/10.1038/s41561-023-01150-](https://doi.org/10.1038/s41561-023-01150-1)
688 1, 2023.

689 Zhang, T. G., Wang, W. C., Gao, T. G., and An, B. S.: Simulation and Assessment of Future Glacial Lake Outburst Floods in the Poiqu
690 River Basin, Central Himalayas, *Water*, 13, <https://doi.org/10.3390/w13101376>, 2021.

691 Zhang, T. G., Wang, W. C., An, B. S., Gao, T. G., and Yao, T. D.: Ice thickness and morphological analysis reveal the future glacial lake
692 distribution and formation probability in the Tibetan Plateau and its surroundings, *Glob. Planet. Change*, 216, 103923,
693 <https://doi.org/10.1016/j.gloplacha.2022.103923>, 2022.

694 Zheng, G. X., Mergili, M., Emmer, A., Allen, S., Bao, A. M., Guo, H., and Stoffel, M.: The 2020 glacial lake outburst flood at Jinwuco,
695 Tibet: causes, impacts, and implications for hazard and risk assessment, *The Cryosphere*, 15, 3159–3180, [https://doi.org/10.5194/tc-](https://doi.org/10.5194/tc-15-3159-2021)
696 15-3159-2021, 2021.